Monitoring of volatile organic compounds (VOCs) in the urban atmosphere of Oslo

Markus Sørensen

Thesis for a Master's
Degree in Chemistry

60 credits

Department of Chemistry
Faculty of Mathematics and Natural Sciences

UNIVERSITY OF OSLO

June 2021

Monitoring of volatile organic compounds (VOCs) in the urban atmosphere of Oslo

2021

Title: Monitoring of volatile organic compounds (VOCs) in the urban atmosphere of Oslo

Author: Sørensen, Markus

http://www.duo.uio.no/

Printed at Reprosentralen, Universitetet i Oslo

Abstract

Volatile Organic Compounds (VOCs) are known precursors in the formation of ground-level ozone and particle matter (PM), both detrimental to human health. While the reduction in air quality induced by traffic emissions has been strictly monitored in the last decade, very few reports exist on the presence of VOCs in Oslo. Furthermore, little is known about the possible influence the Covid-19 pandemic might have on the ambient atmospheres. High-frequency measurements of ambient air of were conducted over a 2.5-month period of cold temperatures centrally located in Oslo to investigate temporal variations of a selection of VOCs. Positive Matrix Factorization (PMF) was subsequently used to model the contributions of the most prominent sources of VOCs. The model revealed VOC contributions of wood combustion were comparable to traffic, in addition to unexpectedly high levels of alcohols related to disinfectants, amounting to nearly half of the total VOC profile in Oslo. The observations were in accordance with recent research suggesting non-traffic sources have increased in significance following the improvement of fuel-based engines and the transition to an electrical traffic fleet.

Preface

I want to extend the greatest appreciation for my supervisor, Armin Wisthaler, for taking me on as his master student. Thank you for introducing me to the exciting and important world of atmospheric sciences. Your expertise and guidance have been essential in the work resulting in this thesis, and my personal development as a scientist.

I am further grateful for the rest of the team at the atmospheric chemistry group. A huge thanks to the group's senior engineer, Tomas Mikoviny, who tirelessly managed the instrument and happily introduced me theory of PTR-ToF-MS. I thank Felix Piel for helping me out with just about anything. I thank Baptiste Languille, my co-supervisor and occasional coffee partner, for your ever kind demeanor and constructive feedback during the otherwise stressful writing process. And while we never collaborated, I thank Alexander Håland, our sole PhD student, for your enthusiastic presentation of group which convinced me to apply there in the first place!

I want to thank Nils Ledermann, who provided us with the perfect measurement's location at the OsloMet University. Without your aid the project would surely turn out quite differently.

A special thank you to my special person, Elisabeth Syse, for being my pillar of support and ideal study partner during the whole master. Finally, a warm thank you to my family and friends for the much-needed emotional support, especially during the Covid-19 lockdown.

Table of Contents

Abbreviations

ABL	Atmospheric boundary layer
BTEX	Benzene, Toluene, Ethylbenzene, Xylenes
CAPS	Cavity attenuated phase shift
cps	Counts per second
C_8, C_9, C_{10}	Aromatic compounds containing 8, 9, or 10 carbons
DT	Drift tube
D_5	Decamethylcyclopentasiloxane
HC	Hydrocarbons
LCU	Liquid calibration unit
LOD	Limit of detection
MEK	Methyl Ethyl Ketone
MS	Mass spectrometry
ncps	Normalized counts per second
NILU	Norwegian Institute for Air Research
OEL	Occupational Exposure Limit
OsloMet	Oslo Metropolitan University
OVOC	Oxygenated volatile organic compound
PA	Proton affinity
PAH	Polycyclic aromatic hydrocarbon
PM	Particulate matter
PMF	Positive Matrix Factorization
ppbV	Parts-per-billion (10^{-9} v/v)
pptV	Parts-per-trillion (10^{-12} v/v)
PTFE	Polytetrafluoroethylene, Teflon
PTR	Proton-transfer-reaction
ToF	Time-of-flight
VCP	Volatile chemical product
VMR	Volume mixing ratio
VOC	Volatile organic compounds

1. Introduction

The economic and population growth during the last two centuries have been the most important driving forces to air pollution (Edenhofer et al., 2014). In 2018, 55 % of the world population lived in urban areas, with around one in eight living in megacities with more than 10 million people (DESA, 2019). Furthermore, urban land cover was expected to expand by 56 – 310 % between 2000 – 2030, emphasizing this trend (Edenhofer et al., 2014). The continuing growth in population, urban development, and infrastructure consequently leads an increase in traffic, energy demand, and general consumption, resulting in an agglomeration of various gaseous pollution sources which may severely impact the ambient air quality. Excessive ambient air pollution can reduce the quality of life by smog formation, cause respiratory issues, and in worst case result in premature deaths. The International Agency for Research on Cancer states that substantial levels of airborne particulate matter below 2.5 µm ($PM_{2.5}$) and ground-level ozone (O_3) rank as the fifth highest cause of death in 2017 (Wild et al., 2020). While pollution of inorganic gases such as NO_2, SO_2, and CO_2 are well characterized, less is known about anthropogenic emissions of the far less abundant Volatile Organic Compounds (VOCs).

1.1 Volatile Organic Compounds (VOCs)

VOC is a collective term for a wide range of organic chemicals which have a sufficient vapor pressure to evaporate at ambient pressure and temperatures. VOCs are present only in "trace amounts", which usually translates to volume mixing ratios (VMRs) in the parts-per-billion (ppbV) range. Nevertheless, they have been shown to be a major contributor to fine particles and O_3 formation in densely populated areas and are fundamentally important in the tropospheric chemistry (Yuan et al., 2017). Many are considered toxic, irritating, or carcinogenic, and are therefore regulated by Occupational Exposure Limits (OEL). An example is benzene, a carcinogen with several anthropogenic sources which has therefore been regulated and monitored for decades (Wild et al., 2020). The short-term and long-term exposure limits for some of the VOCs considered in this thesis are provided in Table A-1 in the appendix.

1.1.1 Urban sources of VOCs

Identification and quantification of the origin of different VOCs is challenging due to the multitude of sources present in an urban environment, which establishes them as an important research objective within atmospheric sciences. A few acknowledged sectors contributing to VOC pollution are discussed in the following chapters.

1.1.1.1 Traffic

Petroleum contains a wide variety of VOCs (EEA, 2018). The aromatics benzene, toluene, ethylbenzene, and xylenes, abbreviated BTEX, are predominantly emitted from traffic and therefore the most renowned tracers for monitoring emissions from this sector. Due to many isomers of the aromatics containing functional hydrocarbon groups, they are commonly denoted according to the number of carbons they are comprised of. E.g., ethylbenzene and xylenes are denoted as C_8-aromatics, trimethylbenzenes and isomers are denoted as C_9-aromatics, and cumene and isomers are denoted as C_{10}-aromatics etc. (Ellis & Mayhew, 2014). This notation is also applied in this thesis. Additionally, NO_x gases are formed by high-temperature combustion mostly associated with diesel engines. The measurement of NO_2 alongside BTEX compounds was crucial to attain a proper overview of the traffic emissions in the ambient measurements (Sousa Santos et al., 2020).

1.1.1.2 Residential wood combustion

Firewood is still widely used for domestic heating in many countries, including Norway. In addition to directly emitting substantial amounts of particulate matter (López-Aparicio et al., 2017), wood combustion is also a considerable source of several VOCs. One of the most abundant VOCs emitted from wood combustion is acetic acid, which is an important atmospheric acid and may thus be involved in gaseous acid-base reactions. Combustion of biomass is a source of benzene alongside traffic emissions (Bruns et al., 2016), in addition to polycyclic aromatic hydrocarbons (PAH), another set of toxic VOCs and known carcinogens (Tsai et al., 2001; Wild et al., 2020).

Residential wood combustion generally increases when ambient temperatures drop, consequently elevating VOC emissions from this sector. Studies from Paris have shown that VOC contributions from residential wood combustion can explain more than 45 % of the overall VOC emissions during the winter season (Baudic et al., 2016; Languille et al., 2020).

1.1.1.3 Volatile chemical products (VCPs)

VCPs encompasses household products containing organic solvents and is therefore an exceedingly broad term. Additionally, most of the VOCs emitted from VCPs can also originate from other non-VCP sources. Decamethylcyclopentasiloxane (D_5) has been suggested as a tracer compound for personal care products. Otherwise, few dedicated tracer compounds exist for VCPs (Coggon et al., 2018).

VCPs have not garnered attention in atmospheric sciences until recently when McDonald et al. (2018) suggested that VCP emissions have been underestimated in previous atmospheric models of U.S cities, citing the reduction of tailpipe emissions and an increase in population density. Furthermore, emissions from VCPs are estimated to scale with population density and should thus become more important with the development of megacities (Gkatzelis et al., 2021a).

1.1.1.4 Biogenic emissions

Anthropogenic emissions are the dominating source of VOCs when considering the local atmosphere of densely populated areas. However, on a global scale, biogenic emission from the world's forests and oceans are by far the largest contributor of atmospheric VOCs. Biogenic emissions mainly consist of isoprene, a molecule hypothesized to be released from trees to cope with thermal stress, and monoterpenes, signal molecules from vegetation which are commonly applied in and thus associated with fragrance. Emissions of isoprene and monoterpenes are highly dependent on light and temperature, and therefore their emissions are much higher during warmer seasons (Guenther et al., 1995). Since the measurements in this thesis were conducted during the winter in an urban environment, the biogenic contributions of isoprene and monoterpenes are expected to be negligible.

1.2 Overview of field

Historically, Oslo has repeatedly exceeded Occupational Exposure Limits (OEL) for NO_2, which has led to continuous political efforts to reduce tailpipe emissions since 2009 (Sousa Santos et al., 2020). This is especially apparent in the government's goal to transition the traffic fleet of Oslo to green energy carriers by 2025, with electric vehicles amounting to 52.2 % of new passenger cars registered in Norway in 2020 (Fevang et al., 2021). In 2021, the air quality in Norway was reported by the levels of PM, NO_2, SO_2, and O_3, monitored by the Norwegian Institute of Atmospheric Research, NILU, with data available at https://luftkvalitet.nilu.no. However, except for a few reports on the yearly averages of the BTEX compounds, there is a general lack of peer-reviewed VOC data of the urban atmosphere in Oslo. This means only part of the pollution is mapped, and contributions from other sources cannot be precisely estimated.

1.2.1 Seasonal effect

Atmospheric circulation, and thus dispersion of pollutants, are dependent on the thickness of the atmospheric boundary layer (ABL). The ABL is the lowermost part of the troposphere where the atmosphere is affected by the surface of the Earth, resulting in a turbulent, well mixed layer with relatively uniform temperatures and atmospheric content in comparison with higher layers. The thickness of the ABL varies from location to locations based on several parameters, but most importantly the ambient temperature. The remainder of the troposphere is called the "free troposphere". When the ambient temperatures are sufficiently warm in the upper part of the ABL, convection by temperature inversion occurs between the ABL and the free troposphere, providing clean air to the ABL, increasing its thickness. When the ambient temperatures are too low, convection between the layers subsides, resulting in less circulation in the ABL (Akimoto, 2016).

In the summer, diurnal trends are characterized by long daytimes with thicker ABL than during nighttime. However, in the winter, the cold surface temperatures make the convection between the mixed layer and the free troposphere subside much earlier in the day, leading to low circulation for a prolonged time. The result is an ambient atmosphere much more susceptible to accumulation of pollutants near anthropogenic emissions sources, which may lead to reduced air quality in large cities (Akimoto, 2016). Since the measurements in this thesis were performed from November to February, the VMRs of anthropogenic VOCs were therefore anticipated to be elevated.

1.3 Aim of thesis

Oslo is an interesting location for conducting atmospheric VOC measurements based on the lack of research in the area, the relatively cold environment which promotes accumulation of pollutants, and the high presence of electric vehicles providing an environment with expectedly low VOC contribution from the traffic sector. Furthermore, the measurements were conducted during the Covid-19 pandemic. Various degrees of lockdown were passed over the course of the campaign, which could impact the level of activity and therefore anthropogenic emissions reliant on human routines. Particularly, monitoring VOCs which could be tied to the elevated usage of disinfectants is of high interest as it provides another source of OVOCs otherwise not observed in considerable amounts the ambient atmosphere.

To summarize, this thesis aims to answer three scientific questions:

1) How does the atmosphere in Oslo compare with other big cities in terms of VOC levels?
2) What are the main contributors to VOC pollution in Oslo today?
3) Does the Covid-19 pandemic have an impact on the ambient atmosphere?

2. Method

2.1 Site description: Oslo Metropolitan University

The measurements were initiated at the Oslo Metropolitan University (OsloMet) on 11.11.2020 and continued until June. The measurements period considered in this thesis, however, spanned from 14.11.2020 – 31.01.2021. The delayed start is due to instrumental changes done at the site during the first couple days of setup, leading to incoherent timelines. Various degrees regulations regarding the Covid-19 pandemic were enforced during the campaign, reducing the usual attendance at the University. Additionally, human activity was expected to drop during the Christmas season.

OsloMet is centrally located, close to the royal castle and Karl Johan, Oslo's main shopping avenue. Trafficked streets surround the building, including a tram line (Fig. 2-1).

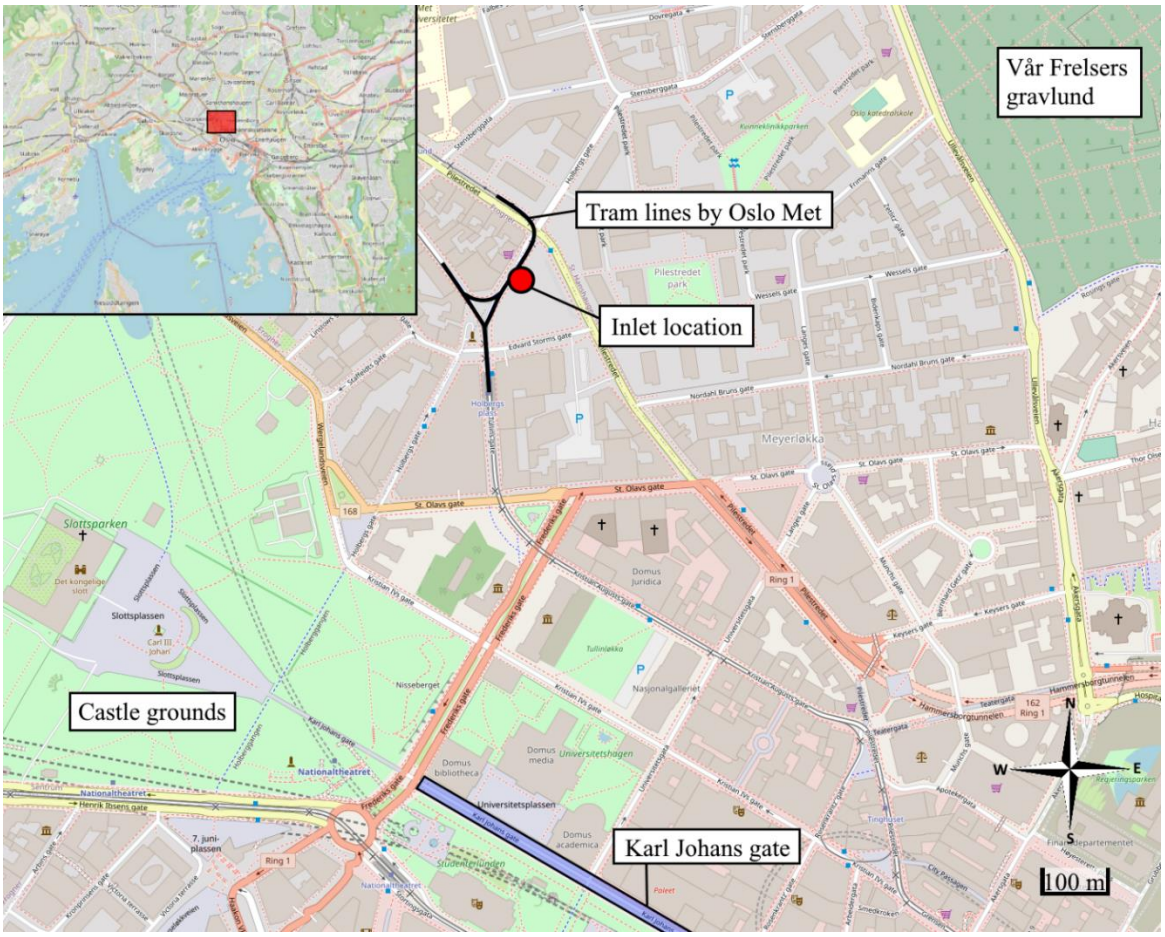

Figure 2-1: Local map of the area around OsloMet with surrounding areas of interest. The smaller map in the upper left corner displays the location in an overview of Oslo City. Map is produced through https://www.Openstreetmap.org

Proximity to these waypoints may have led to local emissions of BTEX from traffic, and VCPs from personal care products or usage of anti-bacterial agents. The site is close to the Norwegian castle grounds and a graveyard, posing as sources of local biogenic emissions from vegetation. Additionally, the city is surrounded by trees and borders to seawater in the south (Oslofjorden), which is expected to influence the general biogenic levels despite the otherwise urban location.

2.2 Experimental setup

Two instruments were deployed at the site: A Proton Transfer Reaction Time-of-Flight mass spectrometer (PTR-ToF-MS, Chapter 2.3) and a NO_2-analyzer (Chapter 2.4), used for measuring VOCs and NO_2 concentrations, respectively, were installed in a closed-off room at the top floor of the OsloMet building during week 46, 2020. Both instruments were deployed from installation until the end of the campaign, however, due to instrumental maintenance and issues with the measurements, there are varying amounts of data from each instrument. An overview of the data coverage is added in the appendix (A-3 and A-4).

The PTR-ToF-MS and NO_2 sampled ambient air through polytetrafluoroethylene (PTFE) inlet lines, brought outside through a customized outlet drilled to maintain a stable room temperature during the campaign. Outside, the inlets were mounted on a lance extended from the railing outside to sample out of the boundary layer of the building. Rain covers were attached to the ends to prevent droplet suction. The PTR-ToF-MS inlet was covered with a 50 ˚C heated tubing, and the rain cover included a particle filter (Fig. 2-2).

Figure 2-2 Inlet setup at OsloMet. The main inlet of the PTR-ToF-MS is heated (black covering) and equipped with both rain cap and particle filter. The clear inlet is connected to the NO_2-analyzer and only requires the rain cap.

2.3 VOC measurements using proton transfer reaction – time of flight – mass spectrometer (PTR-ToF-MS)

The PTR-ToF-MS operates at high response times and without the need of any pre-treatment, allowing operators to obtain measurements online (Fig. 2-3). Combined with sufficient peak separation for mass determination, the instrument has proven invaluable as a means for researching temporal VOC levels (de Gouw & Warneke, 2007). The PTR-ToF-MS used in this work was "home-made", with analyzer parts constructed by Ionicon®.

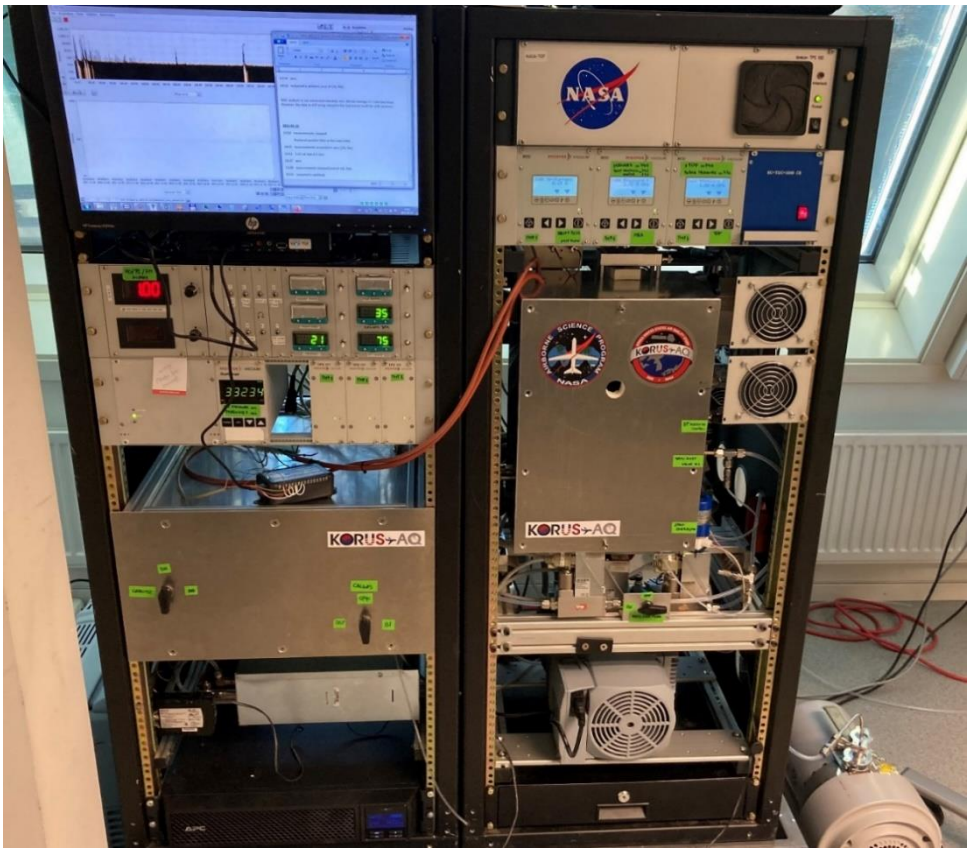

Figure 2-3 Picture of the PTR-ToF-MS set up at OsloMet.

The instrument consists of three main sections: an ion source where proton donors are produced, a drift tube (DT) where sample molecules are protonated, and a time-of-flight mass analyzer, where the ions are separated according to their *m/z* (Fig. 2-4).

In each step, the flight path of the ions increases, making collisions with neutral air molecules more probable. To prevent excessive ion loss, the pressure is reduced by three orders of magnitude (10^{-3}) in each step in what is called *differential pumping* (Yuan et al., 2017).

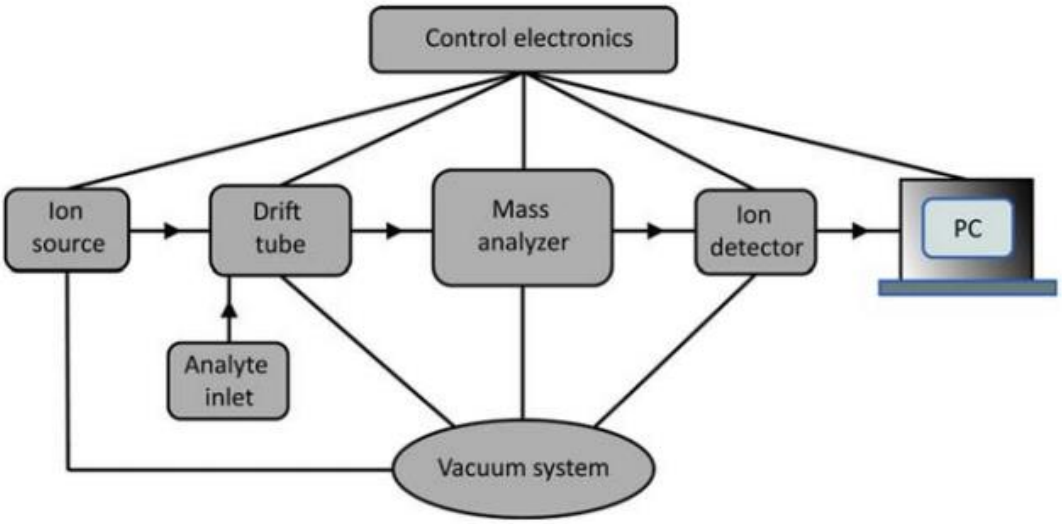

Figure 2-4: An overview of the basic structure of a PTR-ToF-MS (Ellis & Mayhew, 2014).

The following subchapters discuss the working principle of each compartment, as well as how the signals are quantified, in more detail.

2.3.1 Ionization using hydronium-based PTR-MS

Proton-transfer reaction mass spectrometry (PTR-MS) is a chemical ionization technique where a proton is transferred from hydronium ions (H_3O^+) to recipient molecules (M) by the following reaction:

$$H_3O^+ + M \rightarrow [MH]^+ + H_2O \quad (2\text{-}1)$$

The proton donor (here: H_3O^+) is referred to as the "primary ion". Most often the primary ion also includes the cluster, $H_3O^+(H_2O)$, since it amounts to a significant portion of the produced hydronium ions. For the reaction in Eq. 2-1 to be spontaneous, the proton affinity (PA) of the recipient molecule must be higher than that of H_2O. While almost all VOCs exceed the PA (H_2O) = 166.5 kcal/mol, all major constituents of air, i.e N_2, O_2, or CO have a lower PA. PTR is therefore especially useful in analysis of ambient air (de Gouw & Warneke, 2007).

H_3O^+ is formed by passing water vapor through a glow discharge. Electron ionization creates a variety of ions, which are converted into hydronium ions in collisions with neutral water molecules. The resulting ion beam is pure (> 99%), though some contaminants like O_2^+, N_2^+, and NO^+ may form due to back diffusion of air into the ion source (Ellis & Mayhew, 2014).

The primary ions are extracted into the DT, where the analyte sample is introduced. The DT is as a reaction chamber equipped with electrodes, applying an axial potential gradient throughout the DT. The electrical field gradient increases the speed of the ions moving through the DT, limiting the number of collisions, effectively suppressing secondary ion chemistry. Combined with the pressure and temperature parameters of the DT, the field strength is also involved in a parameter called the *reduced electric field*, E/N, reported in Townsend (1 Td = 10^{17} V cm^2). An elevated E/N suppresses the formation of ion clusters by suppressing hydration reactions, however, it increases the fragmentation of formed ions. Operational values ranges from 100 – 140 Td to simultaneously inhibit both mechanisms to an acceptable rate (Yuan et al., 2017).

In this work, the DT was operated at 3.8 mbar pressure, an electric field of 700 V, and was heated to 75 ˚C. The resulting E/N equaled 120 Td, following Eq. B-1 in the appendix.

2.3.2 Mass separation by ToF mass analyzer

The ToF is placed after the DT and is tasked to separate the ions to receive an interpretable mass spectrum. This is done by pulsing packets of ions into a field-free flight region of known length. The accelerating potential (*V*) applied by the extraction pulse imparts the same kinetic energy to all ions, thus ions with different *m/z* will end up with different velocities. The ion's time of flight to is related to its *m/z* by Eq. 2-2 (Gross, 2017).

$$t = \sqrt{\frac{l^2}{2eV} \cdot \frac{m}{z}} \tag{2-2}$$

t = flight time, l = length of flight region

e = elementary charge, m/z = mass-to-charge ratio

V = accelerating potential

During operation, $\frac{l}{\sqrt{2eV}}$ is a constant determined by operational parameters. PTR-MS produces only single charged ions (z = 1), meaning that the *m/z* is equal to the molecular mass of the protonated molecule. According to Eq. 2-2, higher *m/z* results in higher *t* and vice versa. Mass separation is improved by increasing the temporal separation with which two ions of different *m/z* arrive at the detector. This can be achieved by increasing the flight path, *l*.

Modern ToF analyzers contain a reflectron, an electrode stack with a repulsive electric field at the opposite end of the flight region. The reflectron repels the ions back, doubling the flight path, and additionally, the field aids in correcting differences in initial kinetic energies of ions with the same *m/z*. This results in superior peak separation compared to linear ToF analyzers (Ellis & Mayhew, 2014). The instrument used for this thesis is equipped with a reflectron (Fig. 2-5).

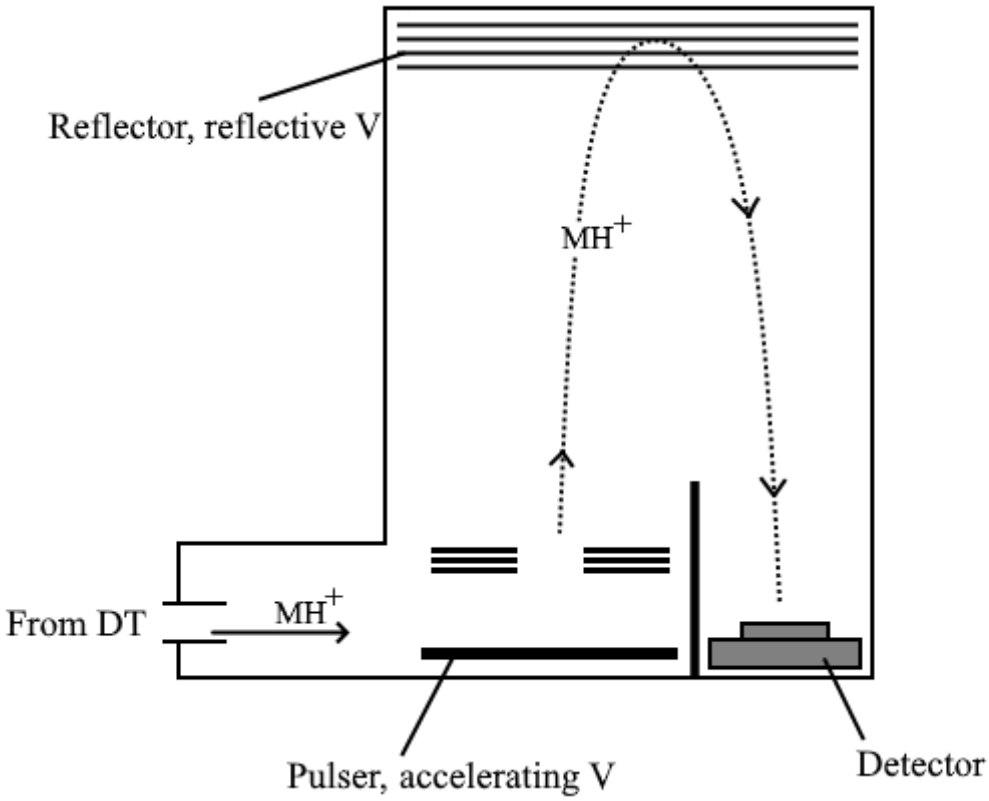

Figure 2-5: Schematic representation of a modern ToF mass analyzer, consisting of a pulser, reflectron, and detector. The ion trajectory is indicated by the dashed line.

2.3.3 Subtraction of background signals

To obtain reference measurements of instrumental background signals, a "zero-air system" was prepared. For these measurements, the ambient air was pulled through a high-temperature, Pt-based catalyst to remove VOCs entering the instrument. The purpose was to subtract the VOC signals in this mode from the analysis of the ambient to eliminate background signals. The zero air was sampled separately through the same inlet as for the NO_2-analyzer, in parallel to the main inlet (Fig. 2-2).

Background measurements were performed once per night through a timed switch that altered which inlet provided air to the drift tube (Fig. 2-6). Background measurements lasted 45 minutes. The starting time of the background measurements was changed once per week to prevent having time intervals without ambient measurements. Starting times varied between 00:00 to 06:00.

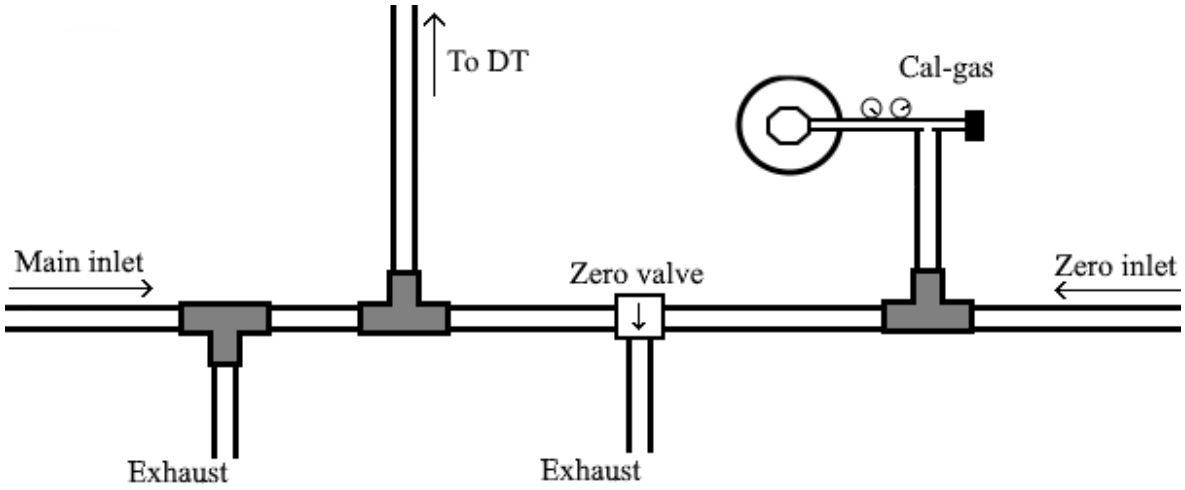

Figure 2-6: Simplified schematic of the combined inlet system for ambient and background/zero measurements.

The complete, detailed setup is presented in the appendix (C-1).

2.3.4 Quantification of PTR-ToF-MS signals

2.3.4.1 Duty cycle correction

Signal intensities in PTR-ToF-MS are recorded in counts per second (cps). The first parameter to consider in the data analysis is the mass dependent *duty cycle*. Duty cycle corrections were performed by multiplying the signals with the following factor (Yuan et al., 2017):

$$d_i = \sqrt{\frac{m/z_{max}}{m/z_i}} \tag{2-3}$$

The mass range was set between 14 – 378 until December 29th, when it was changed to 14 – 450 until the end of the campaign.

2.3.4.2 Normalization

The analyte signals were normalized to the primary ion (H_3O^+ and $H_3O^+(H_2O)$) signals to account for variations in instrumental performance. The adjusted signal intensities are reported in normalized counts per second (ncps), calculated by Eq. 2-4:

$$i(MH^+)_{ncps} = 10^6 \cdot \frac{i(MH^+)}{i\left(H_3{}^{18}O^+\right) \cdot 475 + i\left(H_3{}^{17}{}^+(H_2O)\right) \cdot 769} \tag{2-4}$$

In the mass spectrum, the primary ion peaks are saturated, leading to inaccurate signals. In effect, the peaks are unusable for the analysis. Thus, normalization is performed by using the less abundant ^{17}O and ^{18}O isotopes. These isotope signals are multiplied with the isotopic signals to account for the lower relative abundance in comparison to the ^{16}O isotope. In this thesis, the factor 476 is used for $H_3{}^{18}O^+$, and 769 for $H_3{}^{17}O^+(H_2O)$. 10^6 represents the average magnitude of the summed primary ion signal (Ellis & Mayhew, 2014).

2.3.4.3 Determination of selected sensitivities by calibration

Calibration involves providing known analyte concentrations to determine the instrument sensitivities, given in ncps/ppbV. Thus, VMRs of ambient measurements are obtained by dividing the measured signal for each compound by its respective sensitivity.

Sensitivities for most compounds were determined by using a calibration gas standard (cal-gas) containing 15 VOCs (see A-2). The gas bottle was connected to the zero-air line (Fig. 2-6). Upon use, a set flow of cal-gas was diluted with VOC-free air from the zero-system. By stepwise increasing the cal-gas to zero-air ratio, a calibration curve of measured signal vs. supplied concentration can be generated. The sensitivity corresponds to the slope of the curve. Calibrations were performed on a weekly basis except for the holiday, resulting in a total of 8 separate calibrations.

An exemplary calibration curve with four points performed prior to the campaign is presented in Fig. 2-7. Note that the sensitivity obtained from the slope is not representative for the ambient measurements.

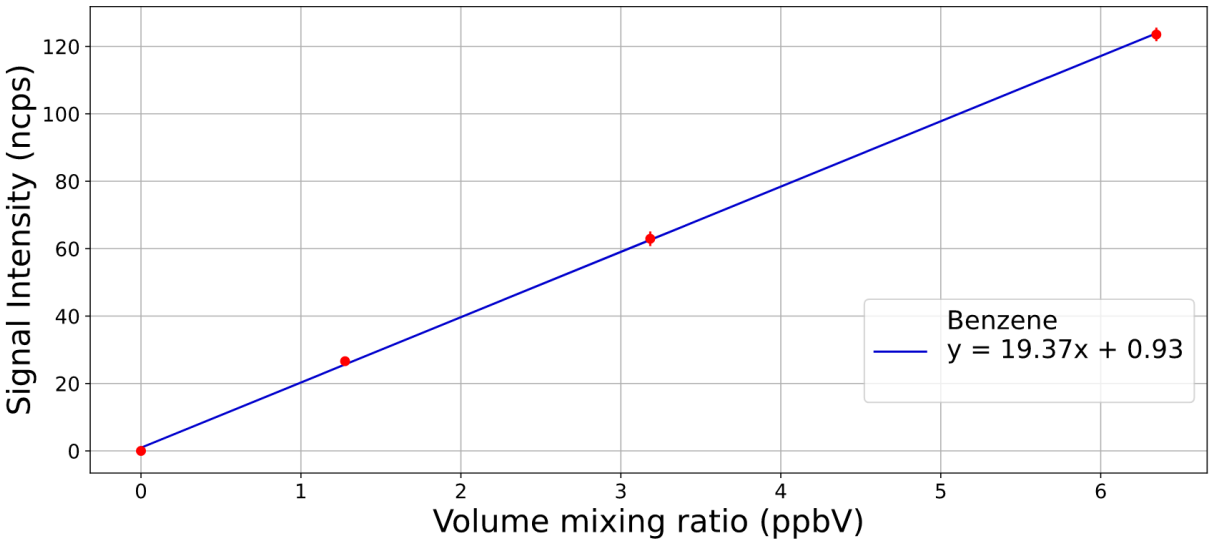

Figure 2-7: Exemplary four-point calibration curve (0 and 5 sccm) of benzene.

The sensitivities will be affected by the instrumental stability, indicated by the primary ion signals. Since a limited number of calibrations were performed during the 79-day campaign, the sensitivities were interpolated on a day-to-day basis between the individual calibrations to obtain a more holistic representation.

Three compounds reported in the results section, i.e. furan, furfural and naphthalene, were not calibrated directly. Since proton transfer occurs at collisional rate, reaction rates (k) can be calculated by ion molecule collision theory (Yuan et al., 2017). With known reaction rates, the sensitivity of a compound (S_i) can be estimated by comparison to a reference compound (S_{ref}), according to the following equation:

$$S_i = S_{ref} \frac{k_i}{k_{ref}} \tag{2-5}$$

Reaction rates for the three compounds have been reported by Cappelin et al. (2012).

2.3.5 LCU calibration

Alcohols from disinfectants, i.e., ethanol and 1- or 2-propanol, showed a major contribution to the urban VOC budget (see 3.2.1). However, those compounds are not present in the cal-gas and alcohols tend to fragment heavily in PTR-MS, making quantification via ion-molecule collision theory impossible. For accurate quantification calibration was performed via a Liquid Calibration Unit (LCU), which enables easy creation of calibration standards.

In the LCU, aqueous analyte solution is nebulized and subsequently evaporated in a heated chamber to generate a well-defined amount of gaseous analyte (Ionicon, 2021). Samples of ethanol, 2-propanol, and 1-propanol were diluted in HPLC water to 10 ppbV solutions provided to the LCU in controllable flows. By varying the liquid flow of the samples to 10 µl/min, a calibration curve could be plotted in the same manner as for the cal-gas calibrations. In contrast, the LCU calibration was only performed once, by the end of the campaign. A complete walkthrough of the sample preparation is provided in the appendix.

2.3.5.1 Humidity-dependence

Sensitivities for most VOCs exhibit a certain dependence on the ambient humidity levels, as some VOCs do not react with the $H_3O^+(H_2O)$ cluster due to its higher PA (de Gouw & Warneke, 2007). The humidity-dependence is especially important for the alcohols, which exhibit large variations in the fragmentation ratios depending on the humidity.

To investigate the humidity dependence of the VOCs, a constant VOC concentrations and variable amounts of water were supplied via the LCU. The water flow was changed stepwise from 0 to 10 µl/min while the cal-gas flow was kept constant at 10 sccm. The instrumental response was plotted against $H_3O^+(H_2O)$ / H_3O^+, a proxy for humidity. An example with benzene is shown in Fig. 2-8:

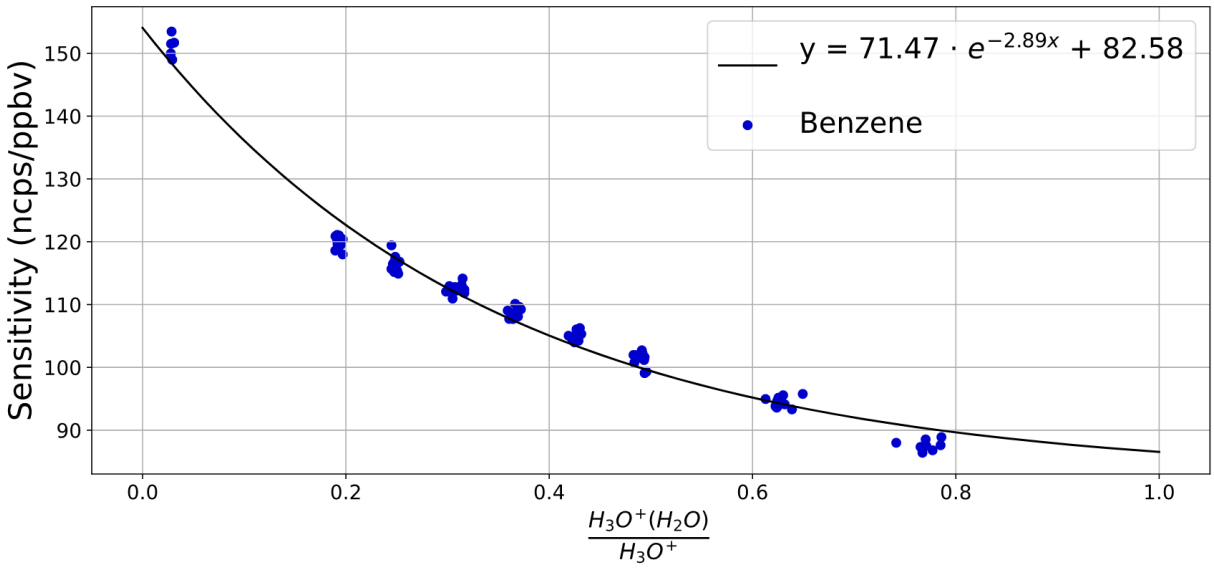

Figure 2-8: Humidity-dependent calibration of benzene.

The humidity-dependence obtained by the LCU calibration of the VOCs were included in the final analysis by scaling according to the sensitivities from the LCU and sensitivities obtained for every day after the interpolation (Chapter 2.3.4.3).

2.3.5.2 Identification of propanol in the ambient measurements

Both 1- and 2-propanol fragment heavily and almost no signal is recorded at the protonated molecule peak. Thus, the fragment ion peaks must be utilized to quantify propanol. The most intense fragments occurred at *m/z* = 41.039, corresponding to $C_3H_5^+$, and *m/z* = 43.054, corresponding to $C_3H_7^+$. The ratios between these two fragments obtained from the LCU calibration of 2-propanol is presented in Table 2-1:

Table **2-1**: Humidity dependent fragment ratios of 2-propanol obtained from LCU-calibration.

	Humidity proxy: $H_3O^+(H_2O)$ / H_3O^+ - ratio				
	0.2	0.4	0.6	0.8	1.0
$C_3H_7^+$ / $C_3H_5^+$	0.99	1.05	1.10	1.15	1.20

2-propanol and 1-propanol exhibit comparable humidity dependence and fragment ratios and could therefore not be differentiated. Hence, the results section will abbreviate the signals as "Propanol", representing what is likely a mixture of both 1-propanol and 2-propanol.

Since propanol is expected to correlate with ethanol (discussed in the results), the alcohols were compared to the ambient $C_3H_7^+/C_3H_5^+$-ratio to investigate if $C_3H_5^+$ is a good proxy for propanol. Fig. 2-9 shows the $C_3H_7^+/C_3H_5^+$-ratio during an event of high signals of ethanol and $C_3H_5^+$.

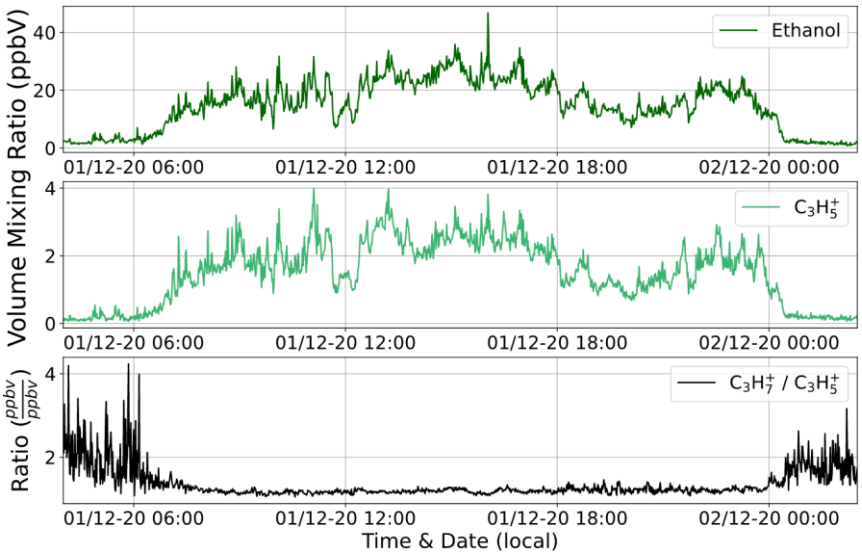

Figure 2-9 Comparison of ambient signals of ethanol, $C_3H_5^+$, and the ratio of propanol fragments. Local time is UTC+1.

The observed ratio of $C_3H_7^+/C_3H_5^+$ was comparable with the ones obtained from the LCU-calibration with 2-propanol (Table 2-1) during the high daytime signals. Therefore, the $C_3H_5^+$ signal was considered appropriate for approximating the propanol VMR.

2.4 NO_2 measurements using CAPS NO_2 Analyzer

The analyzer used in this work to obtain NO_2-data was a Model T500U CAPS NO_2-Analyzer from Teledyne API. Its measurement principle is based on optical absorption spectroscopy, directly measuring ambient NO_2 down to ppbV levels by Beer's law (B-2).

The instrument consists of a rectangular chamber in which ambient air is introduced. An ultraviolet light emitting diode located at one end of the chamber emits light centered at 450 nm, the broadband frequency of NO_2. The light eventually reaches a detector on the other end measuring how much of the emitted light intensity was lost during its trajectory, known as the absorbance (Fig. 2-10).

The Cavity Attenuated Phase Shift (CAPS) method relies on alterations in the path length of the light for precise measurement of the absorbance. The path length is drastically increased by two reflective 450 nm mirrors located inside the chamber. However, the path length is cut short with the presence of NO_2, inducing a pronounced, concentration-dependent shift in the detected signals. By creating spectrums of the signals over short time-intervals (µs), the ambient concentrations of NO_2 are calculated at a 1 Hz frequency. The instrument automatically converts the signals to ppbV (TAPI, 2014).

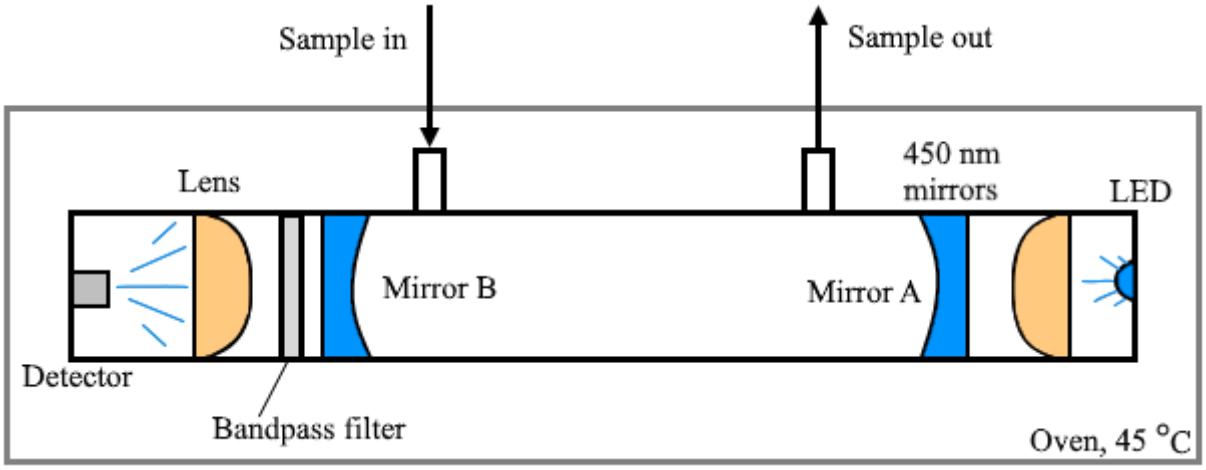

Figure 2-10: The measurements chamber of the CAPS NO_2-Analyzer. Two reflective mirrors extend the path length of the ultraviolet light emitted from the LED to the detector. Ambient air is continuously flowing through the system, and the various NO_2 concentrations present will cut the path lengths short, creating a signal shift which the instrument converts to ppbV levels. The chamber is surrounded by an oven to keep the temperature constant and prevent formation of droplets.

In addition to the analyzer, an external Teledyne Model 751 Zero Air generator was used for background measurements (Fig. 2-11). The generator contains a NO_2 scrubber, providing air free of NO_2 within scheduled times. A timer activated the generator every night for two hours; one hour warm-up, 30 min zero-, and 30-min cooldown. As with the PTR-ToF-MS, scheduled times was changed once a week to not have the same time intervals without ambient measurements. The generator pulled air from its surroundings and was connected directly to the NO_2-analyzer. The setup is included in the complete schematic in C-1.

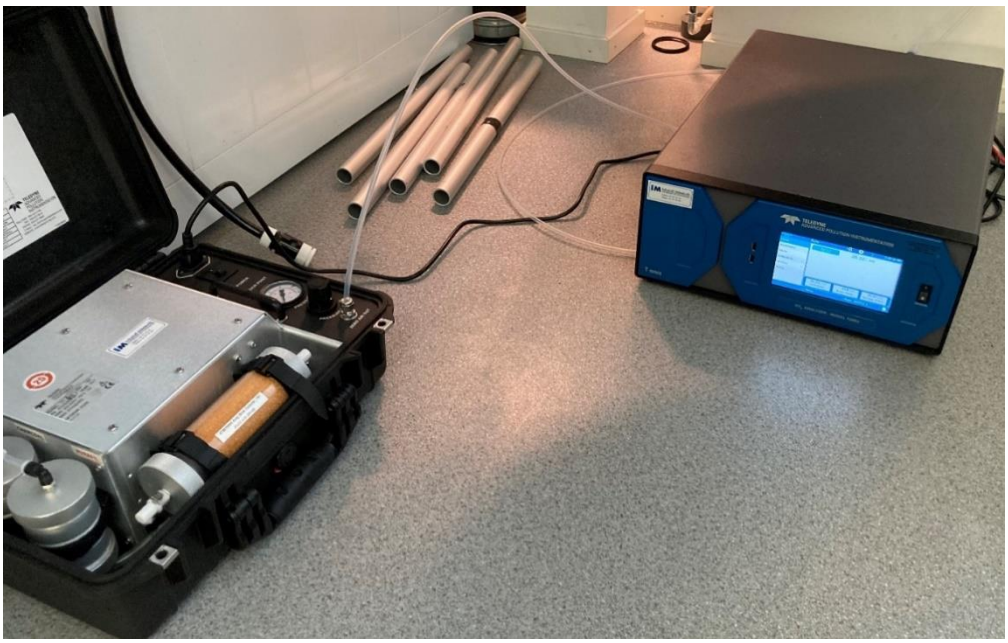

Figure 2-11: The NO2-analyzer (right) and its zero-air system (left) installed at OsloMet.

2.5 Data acquired from external sources

The Norwegian Public Roads administration, Statens Vegvesen, has (as of May 2021) several stations alongside roads in Oslo measuring the number of cars passing per hour. This data, available to the public, was downloaded from https://www.vegvesen.no/trafikkdata. The station closest to OsloMet, called “Vaterlandstunnelen”, was chosen for the analysis.

Ambient temperature data from the Metereological institute of UiO was used. This data was accessed with code through their online database: https://www.frost.met.no.

The locations of the external measurement stations are shown in Fig 2-12.

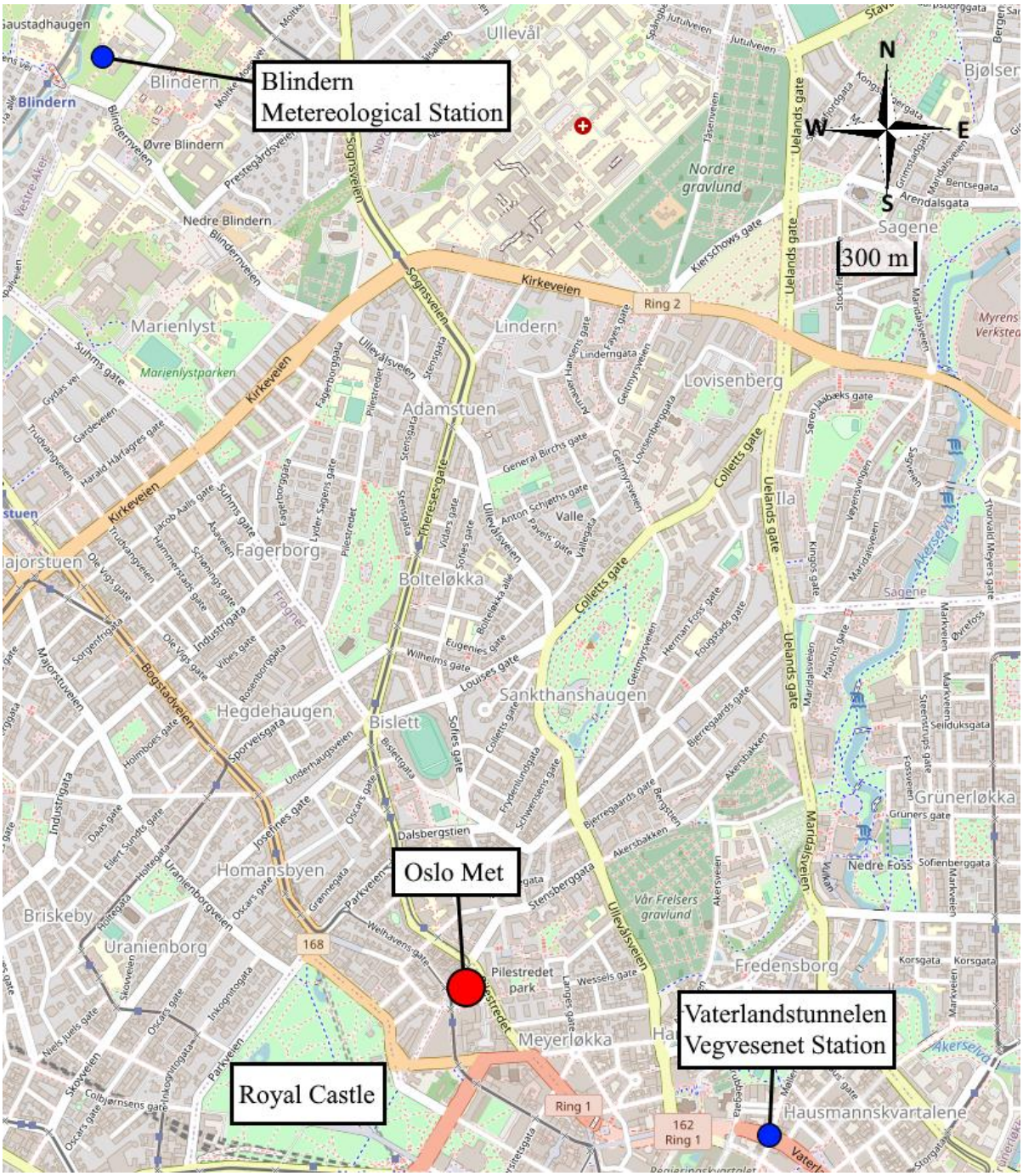

Figure 2-12: Locations of measurements stations of external sources (blue) relative to the OsloMet site (red). Map is produced through https://www.Openstreetmap.org

2.6 Positive Matrix Factorization

The Positive Matrix Factorization (PMF) model is a free software developed by the U. S Environmental Protection Agency to quantify the contribution of various sources of a chemical dataset (Norris & Duvall, 2014). PMF studies have been utilized extensively for apportion of VOCs, including the research employed for comparisons in this thesis (Baudic et al., 2016; Gkatzelis et al., 2021b; Languille et al., 2020; Rantala et al., 2016).

The initial PMF model was developed over 20 years ago, and first described by Paatero and Tapper (1994). The fundamental mathematical principle is summarized in Eq. 2-6:

$$X = G \cdot F + E \tag{2-6}$$

Where X is the provided data matrix split into factor contributions (G), factor profiles (F), and residuals (E). The operator must set a selected number of factors to consider and subsequently interpret which sources the resulting factor profiles correspond to. Therefore, it is critical to identify an optimal number of factors to cover all sources within reason for the sample set (Norris & Duvall, 2014).

In addition to a data set, the operator must provide a table with uncertainties in the exact same format as the chemical dataset. Following the procedure of Ito and al. (2004), the uncertainties were approximated by adding 5 % of the values in the ambient measurements data to the Limit of Detection (LOD). The LOD is defined as 3 times the standard deviation of the blank measurements, corresponding to the least signal required to separate it from the background noise (Ellis & Mayhew, 2014).

The model cannot operate with negative or missing values, which required pre-treatment of the sample data (Norris & Duvall, 2014). NaN-values tied to instrumental downtime were replaced with a marker value of - 999, which the PMF software could remove automatically. A few negative values occurred for compounds of VMRs just above their LOD after the zero-subtraction process. These values were set to zero in the sample dataset prior to introduction in the PMF software.

Finally, the software was not able to handle the high-frequency, 15-second-acquisition data from the whole campaign. Thus, 1-hour averaged data was utilized for the PMF analysis.

3. Results and discussion

3.1 Auxiliary data

Fig. 3-1 presented the meteorological data and traffic data used to aid the interpretation of the results.

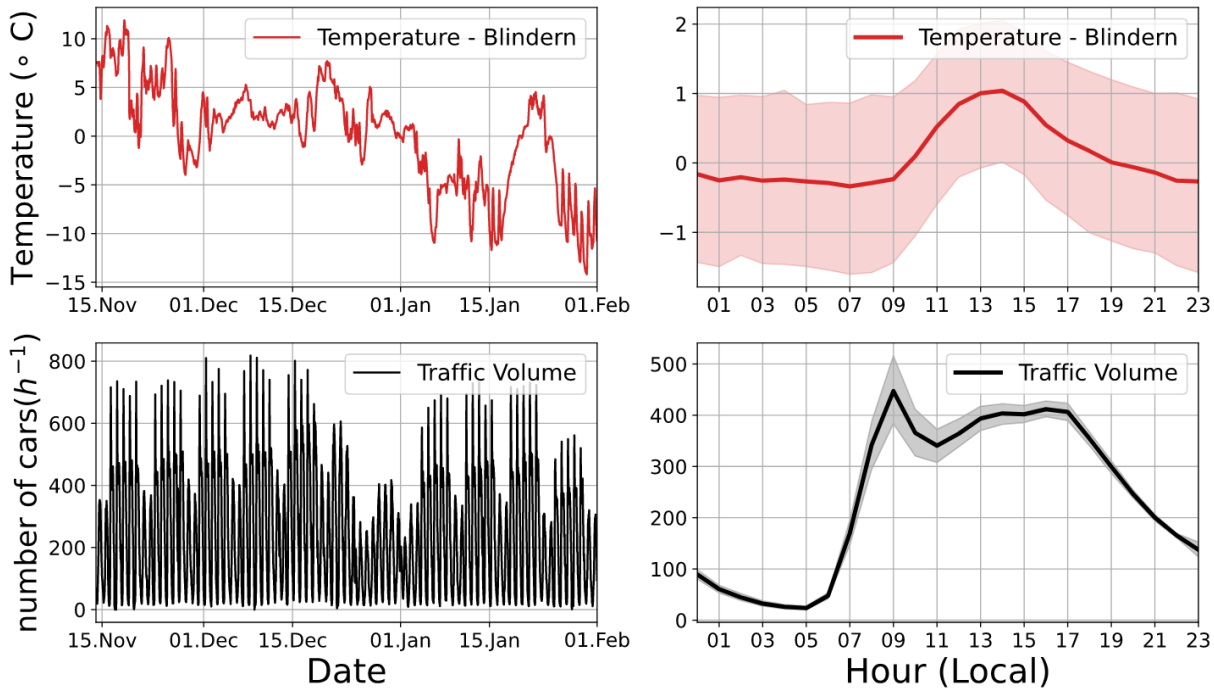

Figure 3-1: Time series (right) and average diurnal (left) of ambient air temperature and traffic volume. Local time is UTC+1.

Ambient air temperatures were mostly above 0 °C in the early phase of the measurement campaign, i.e. in November and December of 2020. An extended period with temperatures below -5 °C occurred in January 2021. The average diurnal profile of air temperature shows the expected increase during the short sunshine hours in Oslo in winter, with a stable temperature profile during the dark hours. The large confidence intervals reflect the large temperature shift over the course of the campaign.

The traffic data show a remarkably stable traffic volume during the weekdays and periodic drops during the two weekend days. This pattern was interrupted by the Christmas and New Year's holidays, when the traffic volume exhibited a significant drop. The decrease in traffic volume during the last week in January remains unexplained.

3.2 Target VOCs

PTR-ToF-MS mass spectra are complex and typically include hundreds of m/z-signals in ambient air. For this Master's project, I selected 16 target VOCs to be analyzed. The target VOCs include pure hydrocarbons (HCs) consisting of only carbon and hydrogen atoms, oxygenated VOCs (OVOCs) consisting of carbon, hydrogen, and oxygen atoms and one siloxane consisting of carbon, hydrogen, oxygen, and silicon atoms. The target VOCs are well measurable by PTR-ToF-MS, they are important from an air quality point of view, and they include tracer compounds which can be used for source apportionment studies. Table 3-1 summarizes the results from a statistical analysis of the target VOC data. The data are reported as VMRs in ppbV.

Table 3-1: Results from a statistical analysis of the target VOC data (in ppbV).

VOC Classes		Compound	Mean	Median	Maximum	σ
Pure HCs	Aromatics	Benzene	0.28	0.25	1.82	0.18
		Toluene	0.22	0.18	3.42	0.17
		C_8 aromatics*	0.18	0.13	2.75	0.15
		C_9 aromatics*	0.07	0.05	1.78	0.06
		C_{10} aromatics*	0.04	0.03	0.56	0.04
		Naphthalene	0.05	0.04	0.51	0.05
OVOCs	Alcohols	Methanol	1.49	1.18	11.53	1.07
		Ethanol	4.86	3.28	81.15	5.06
		Propanol*	0.79	0.57	19.31	0.75
	Carbonyls	Acetaldehyde	0.70	0.50	5.14	0.62
		Acetone/Propanol	0.62	0.50	12.73	0.42
		Methyl Ethyl Ketone	0.15	0.11	3.82	0.12
		Furfural*	0.13	0.06	2.20	0.19
	Others	Acetic Acid	1.10	0.67	14.40	1.29
		Furan	0.10	0.05	1.68	0.14
Siloxane		D_5	$23 \cdot 10^{-3}$	$19 \cdot 10^{-3}$	$21 \cdot 10^{-2}$	$21 \cdot 10^{-3}$

* Sum of all isomers

3.2.1 Alcohols

Fig. 3-2 presents the time series and average diurnal plots of the three alcohols (methanol, ethanol, propanol) investigated in this study. Methanol exhibited an evening peak, with VMRs starting to increase at 16:00 and peaking at around 20:00. Methanol is known to be abundantly formed when wood is burned (Bruns et al., 2016). Residential wood burning is a common practice in Oslo, and the methanol time profile can be explained with the firing of woodstoves during the evening hours.

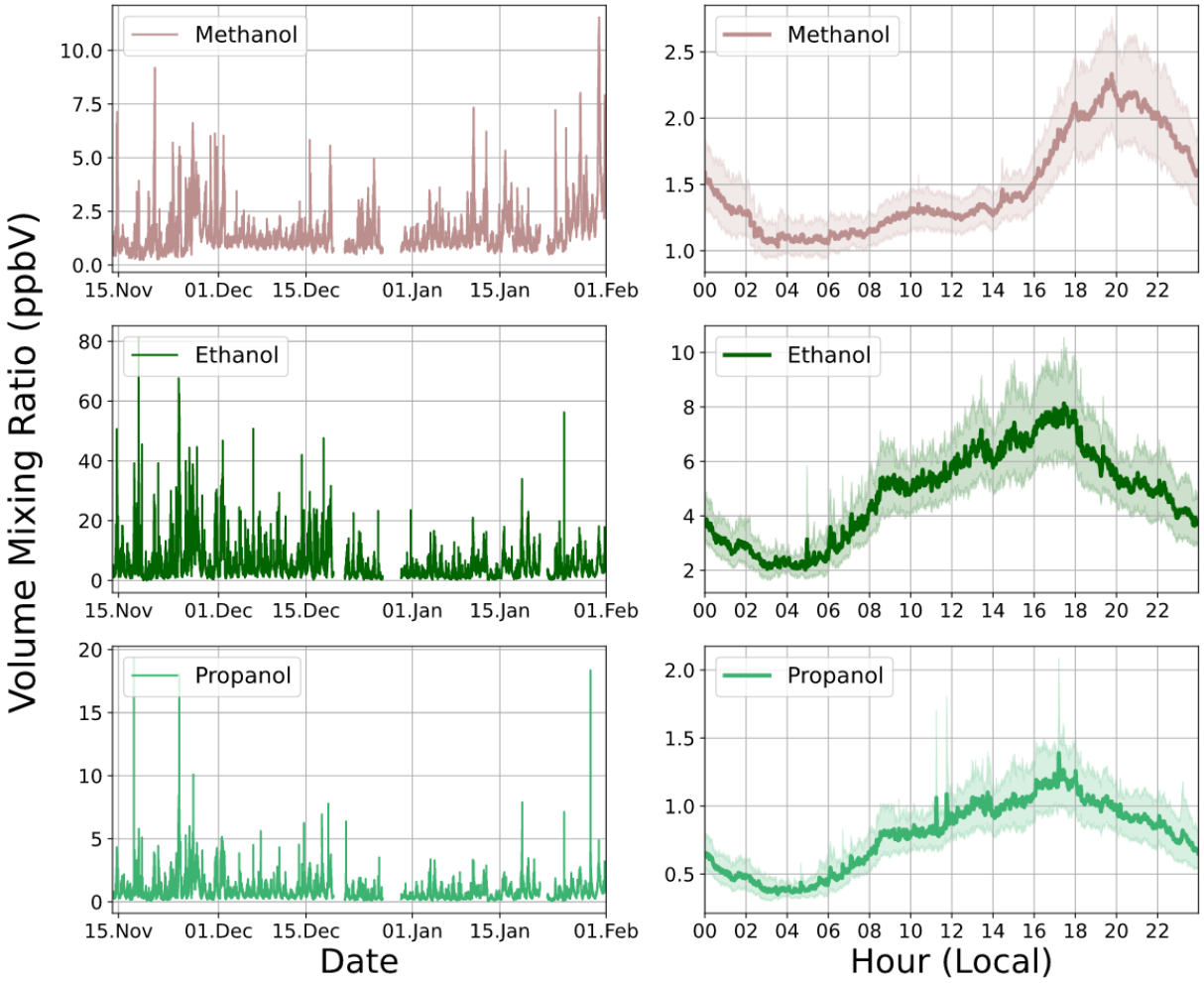

Figure 3-2: Time series (left) and average diurnal profiles (right) of the VMRs of included alcohols (1-min data averages)

The time series of ethanol and propanol shows unexpectedly high VMRs (tens of ppbVs). The plots of the average diurnal profiles show that the two alcohols gradually built up during the day, reached a maximum between 17:00 and 18:00 and gradually declined overnight.

The two alcohols exhibit a similar diurnal profile, indicating a high level of correlation. This was confirmed in the propanol *vs.* ethanol scatter plot shown in Fig. 3-3. While correlations need to be interpreted with caution, the high regression coefficient ($R^2 = 0.87$) suggests that the two alcohols arise from a common source.

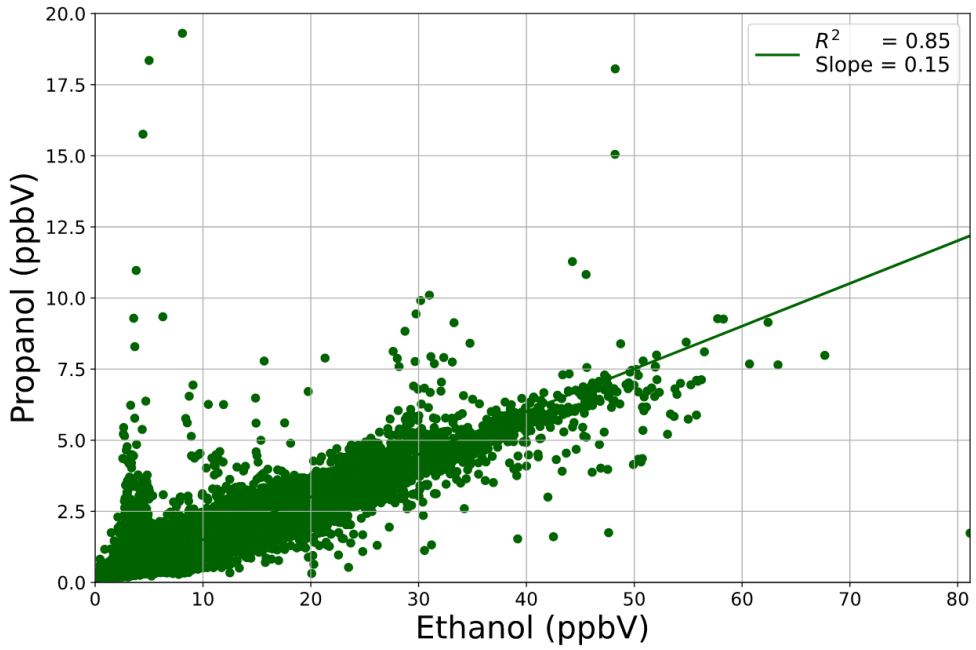

Figure 3-3: Propanol *vs.* ethanol regression plot (1-min data averages).

In Norway, hand and surface disinfectants mainly consist of ethanol, with minor amounts of 1-propanol or 2-propanol added. The measurement campaign took place during the Covid-19 pandemic when disinfectants were widely used. Since alcohols are highly volatile, it is reasonable to assume that most of the alcohols applied onto surfaces and hands evaporated and built up in the atmosphere. Consequently, ethanol became the dominant VOC in Oslo's urban atmosphere. Unfortunately, no atmospheric alcohol data are available for Oslo from pre-Covid times to confirm the increase in ethanol and propanol levels during the pandemic. Rantala et al (2016) did, however, measure alcohols during wintertime in Helsinki in 2015, reporting a median methanol VMR of 1.13 ppbV and a median ethanol VMR of 0.82 ppbV. The methanol levels in Helsinki were thus almost identical to those measured in Oslo, while ethanol levels were a factor of 4 lower than in Oslo. Gkatzelis et al. (2021) recently reported a high atmospheric ethanol levels in New York City (NYC). They found a median ethanol VMR of ~7.8 ppbV in 2018, i.e. during pre-Covid times. They also found ethanol to correlate with population density, and since NYC has a factor of 4 higher population density than Oslo (Gkatzelis et al., 2021a; SSB, 2021) higher atmospheric ethanol levels are expected.

A chemical inventory for Manhattan lists pesticides, personal care, cleaning, and coatings as sources of ethanol. This finding indicates that ethanol could be the dominant VOC in the urban atmosphere even without the widespread use of disinfectants. It should, however, be noted that the sensitivity values reported for the PTR-ToF-MS measurements in NYC were much lower than those found in this study. Ethanol is difficult to calibrate, and ethanol levels reported by Gkatzelis et al. (2021) may thus potentially be biased high.

3.2.2 Carbonyls

Fig. 3-4 presents the time series and average diurnals of the four carbonyls investigate in this study. Propanal is an isomer of acetone and the time trace shown is the sum of the two species.

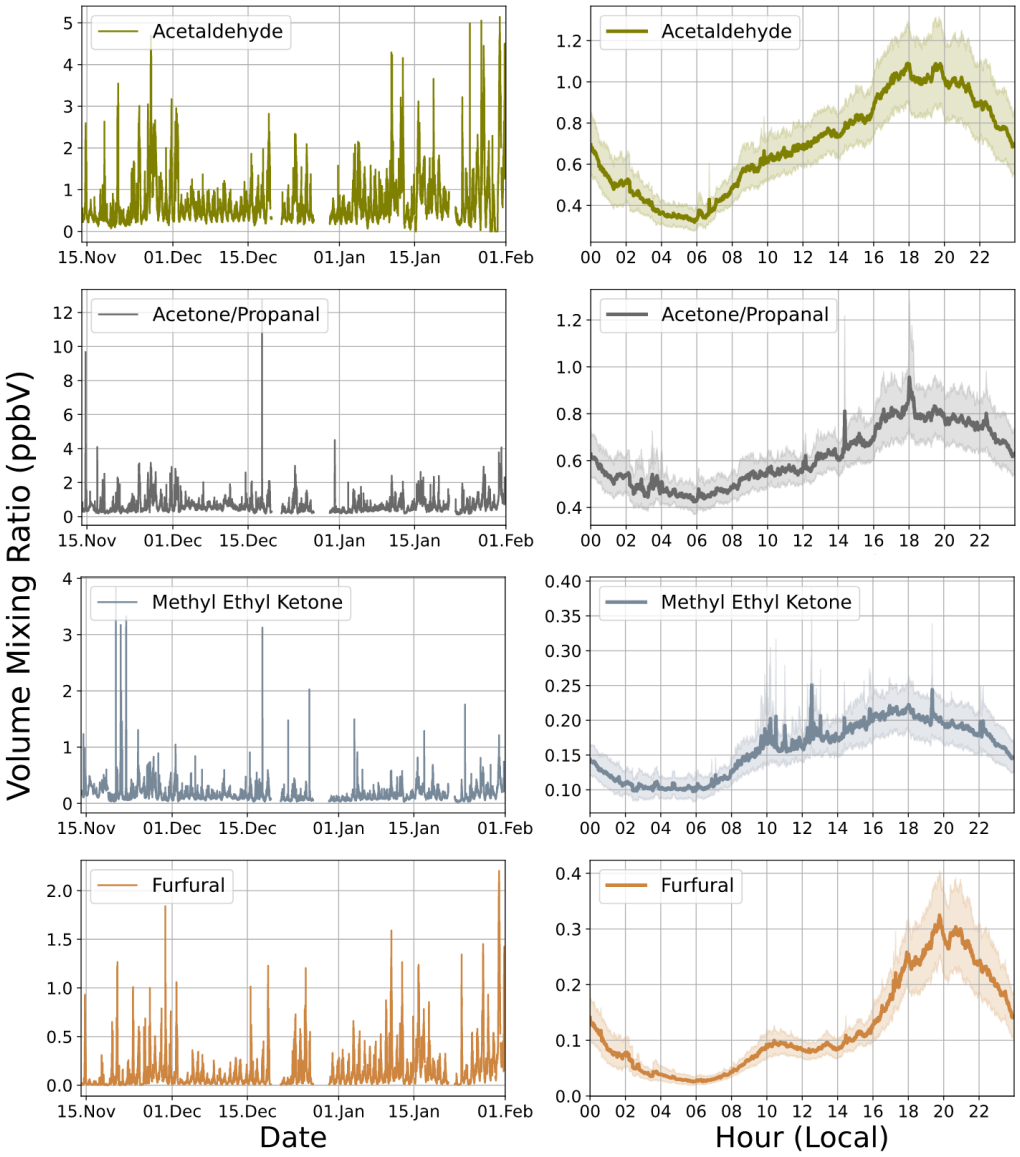

Figure 3-4: Time series (left) and average diurnal profiles (right) of acetaldehyde, acetone/propanal, methyl ethyl ketone and furfural VMRs (1-min data averages)

The average diurnal profile of furfural in Fig. 3-4 is almost identical to that of methanol shown in Fig. 3-2. This finding does not come as a surprise since furfural is specifically emitted from wood burning (Bruns et al., 2016). Acetaldehyde, acetone, and methyl ethyl ketone (MEK) gradually built up during the day, reached a maximum between 17:00 and 20:00 and slowly declined overnight. These carbonyls have a variety of sources including primary emissions from wood burning and traffic (Bruns et al., 2016; Gkatzelis et al., 2021b) and secondary photochemical formation (Wang et al., 1995). The gradual increase during the day may thus be caused by traffic emissions and photochemical formation, while the evening peak may be explained by wood combustion emissions. It is worth noting that the OH-radical induced degradation of ethanol forms acetaldehyde, while the two propanol isomers get oxidized to acetone and propanal, respectively. Given the high VMRs of the precursor alcohols, these carbonyls are thus expected to be formed by OH-chemistry in the atmosphere. The high acetaldehyde VMRs (1.0 ppbV on average, Fig. 3-4) during the evening hours may thus be a caused by the photochemical build-up of acetaldehyde during the day and the additional contribution from direct biomass burning emissions. MEK is sometimes added as a denaturation agent in alcohols including disinfectants.

3.2.3 Other OVOCs

The time series and average diurnals of the two remaining OVOCs, acetic acid and furan, are shown in Fig. 3-5. Acetic acid and furan are known to be strongly and predominantly emitted from wood burning (Bruns et al. 2016). It is thus not surprising that the average diurnal profiles resemble those observed for methanol and furfural.

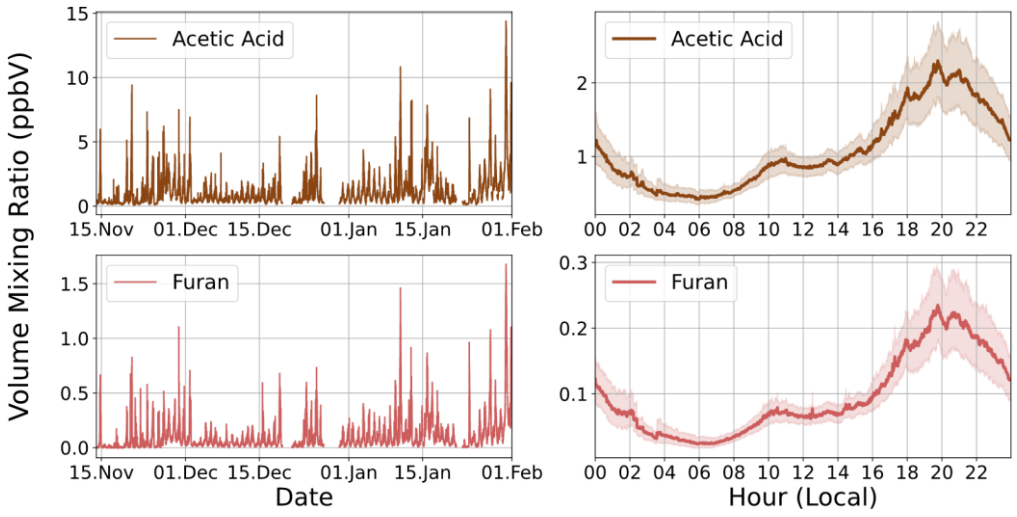

Figure 3-5: Time series (left) and average diurnal profiles (right) of acetic acid and furan VMRs (1-min data averages)

3.2.4 Aromatics

The time series and average diurnals of a series of aromatic VOCs are presented in Fig. 3-6.

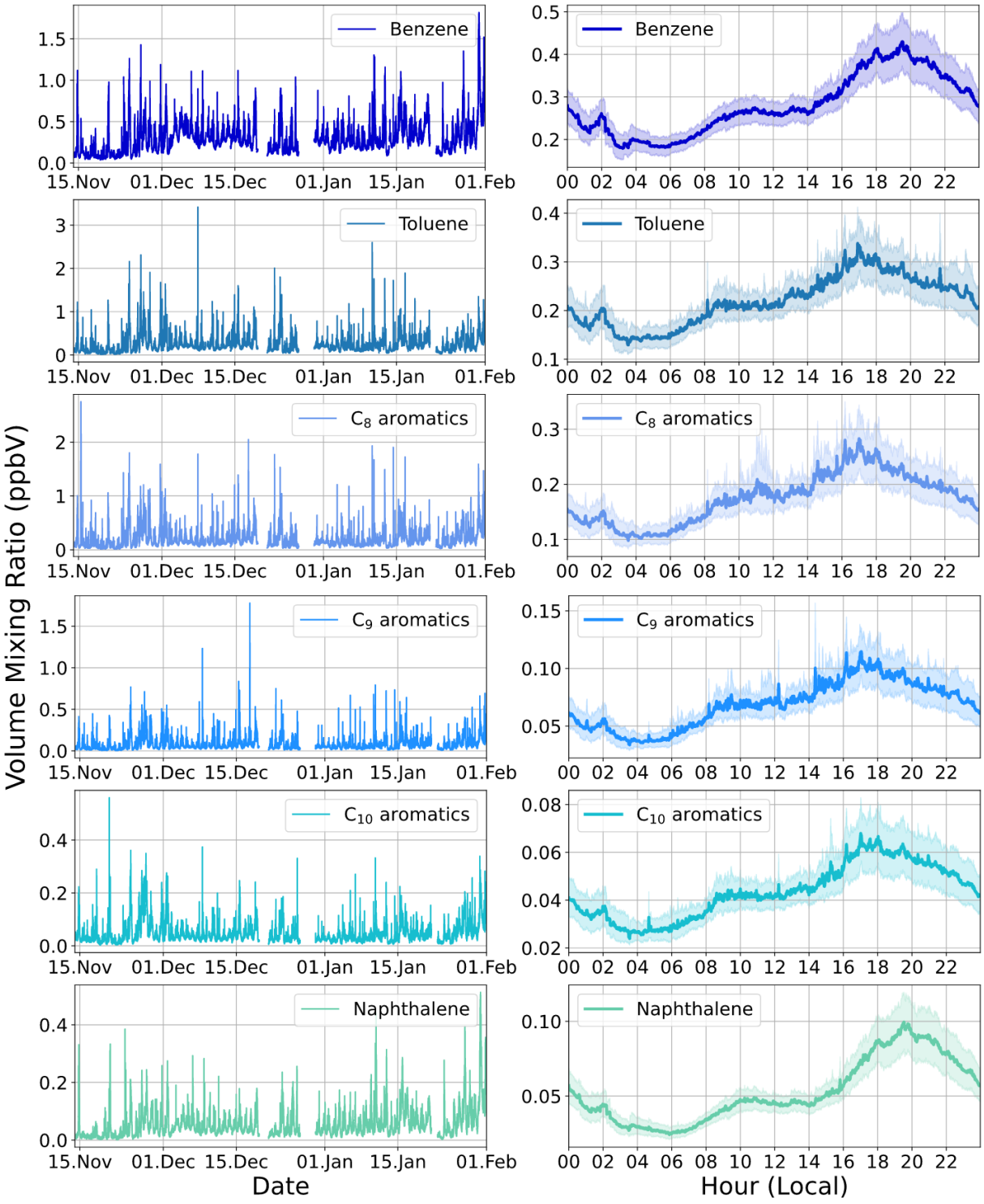

Figure 3-6: Time series (left) and average diurnal profiles (right) of benzene, toluene, C_8 aromatics, C_9 aromatics, C_{10} aromatics and naphthalene VMRs (1-min data averages)

Toluene and the C_8-to-C_{10} aromatics exhibit a similar diurnal profile, with an increase in the morning, stable levels during the day, an afternoon peak between 17:00 and 18:00 and a decline overnight. Benzene and naphthalene exhibit a slightly different temporal behavior, peaking at around 20:00. Aromatic compounds are emitted by traffic and by wood burning, but the latter is known to emit benzene and naphthalene in higher quantities ((Bruns et al., 2016). This is nicely illustrated in Fig. 3-7, a scatter plot of benzene *vs*. toluene color-coded in furfural. There are two predominant branches, an upper branch with a benzene-to-toluene ratio of ~2 and a lower branch with a benzene-to-toluene ratio of ~0.5. The upper branch is rich in furfural and can thus be linked to biomass burning emissions. The lower branch is depleted in furfural and can thus be linked to traffic emissions. The evening peak in the diurnal pattern of benzene and naphthalene can thus be explained by residential wood burning emission, while during the day aromatics are mostly emitted by traffic.

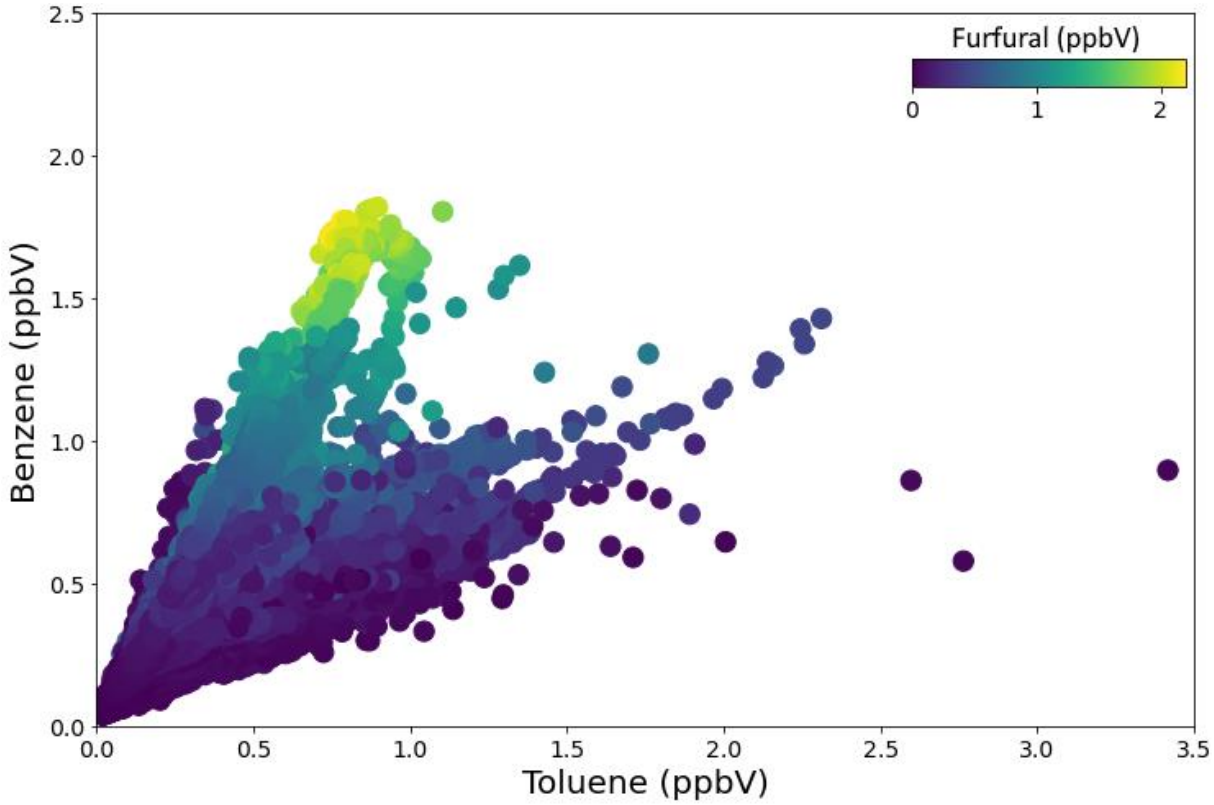

Figure 3-7: Benzene *vs*. toluene scatter plot color-coded in furfural VMRs (1-min data averages)

3.2.5 Siloxane

The time series and average diurnal profile of the D_5-siloxane is presented in Fig. 3-8.

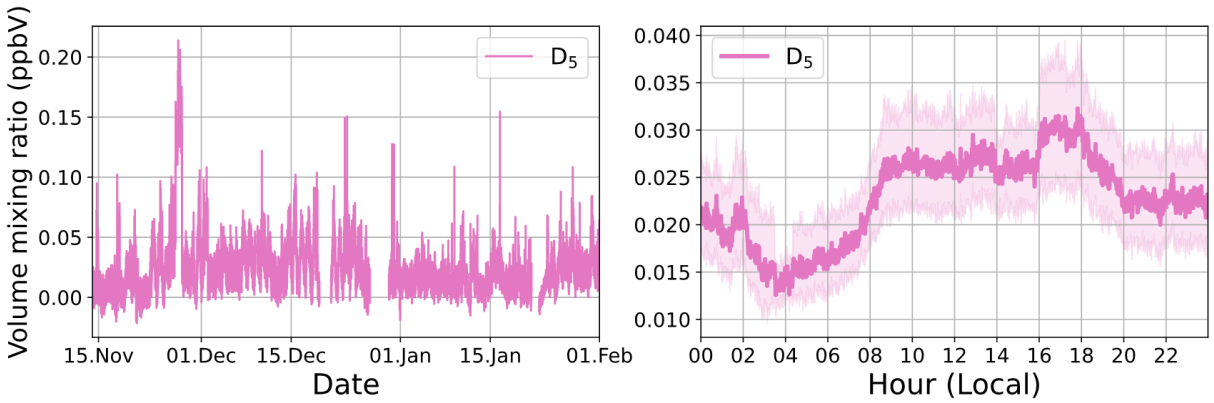

Figure 3-8 Time series (left) and diurnals (right) of D_5-siloxane VMRs (1-min averages)

The observed D_5-siloxane VMRs were typically in the low parts-per-trillion (pptV, 10^{-12} v/v) range. VMRs in the average diurnals ranged from 15 to 30 pptV, which is similar to the 20 pptV median VMR reported for NYC by Gkatzelis et al. (2020). On a few occasions, D_5-siloxane did however exhibit short-term spikes up to 100-200 pptV. Gkatzelis et al. (2020) claimed that the D_5-siloxane is exclusively emitted from personal care products. The use of D_5-siloxane (and D_4-siloxane) in wash-off personal care products was, however, banned in Norway as of 01.02. 2020 (Miljødirektoratet, 2021). The fact that it was still detected in the urban atmosphere of Oslo may indicate that some D_5-containing products are still in use or that other sources may be significant. It is worth noting that the D_4-siloxane was not detected.

3.3 Nitrogen dioxide (NO_2)

NO_2 was measured in addition to the VOCs. The time series and average diurnal profile of NO_2 is presented in Fig. 3-9. The mean NO_2 VMR was 9.0 (± 8.2) ppbV, the median NO_2 VMR was 5.9 ppbV, and the maximum NO_2 VMR was 79.0 ppbV. The average diurnal profile of NO_2 closely resembles the diel profile of traffic volume (Fig. 3-1). A morning rush peak is observed around 9:00 followed by a slight decrease and sustained levels during the afternoon. In the time series, a pronounced drop in NO_2 is observed during the Christmas and New Year's holidays.

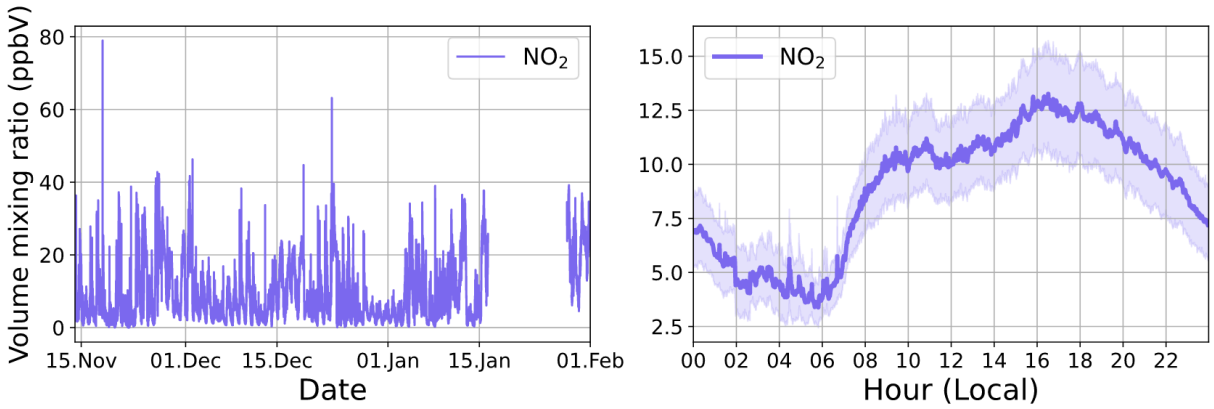

Figure 3-9: Time series (left) and average diurnal profiles (right) of nitrogen dioxide (NO_2) (1-min data averages)

Fig. 3-10 shows 1-hour averaged NO_2 concentrations in units of µg/m^3. The applied ppb-to-µg/m^3 conversion factor is 1.84 (eq. B-3). The hourly limit value for NO_2 is 200 µg/m^3, measured as an average over one hour. The observed NO_2 concentrations were far from reaching the legal threshold. The mean concentration over the whole campaign was 16.33 µg/m^3. In wintertime concentrations are generally higher than in summer due to reduced pollutant dispersion. It is thus anticipated that the yearly average would also be well below the legal 40 µg/m^3 limit.

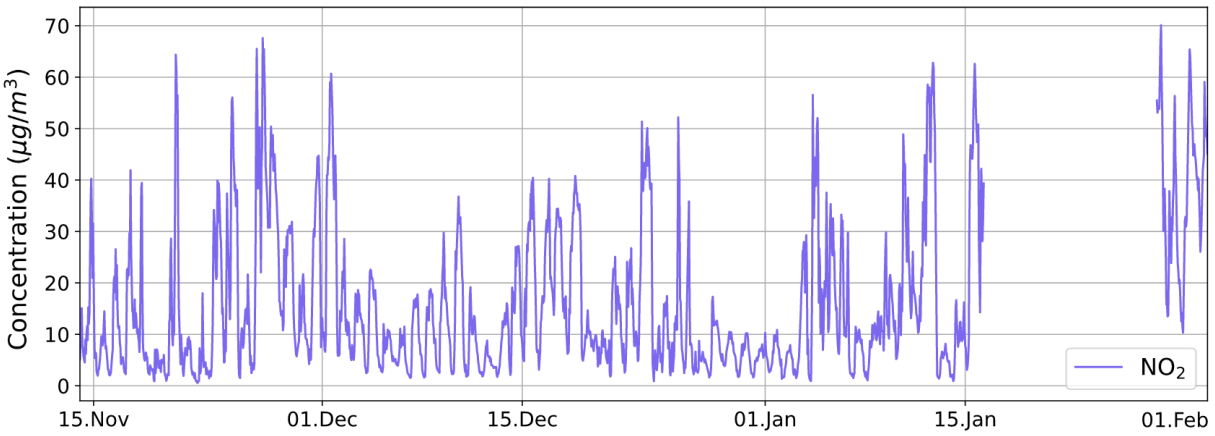

Figure 3-10: Time series of NO_2 data measured by the NO_2-analyzer, converted to µg/m^3. 1-hour averaging

3.4 Source apportionment by PMF

PMF is a multivariate factor analysis tool that is widely used for source apportionment of air pollution (see Methods chapter). It separates the time series of input parameters (VMRs of air pollutants; here: 16 target VOCs) into a manually selected number of factors, representing different sources. A varying number of factors was tested to find the most reasonable solution, which consisted of four source factors. Three sources (traffic, biomass combustion, disinfectants) were already identified from the analyses presented in chapter 3.2. A fourth factor was included to take into account the contribution from aged urban background pollution. This was in accordance with other PMF studies employing similar factor allocation strategies (Baudic et al., 2016; Gkatzelis et al., 2021b). The contribution of the four sources to the 16 target VOCs is shown in Fig. 3-11. The apportionment of the traffic and wood combustion sources appears to be solid; the marker compounds are found in the respective source factor. The long-lived compounds (methanol, acetone, MEK, D_5) exhibit the expected contribution from the background source. A significant fraction of the aromatics is apportioned to the disinfectant source, which may be explained by the fact that more traffic means more mobility and thus more disinfectant use. A better separation might be achieved by applying additional constraints through another software called Source Finder (Gkatzelis et al., 2021b). Such an in-depth analysis was, however, outside the scope of my Master's project. The average diurnal profiles of the four factors are shown in Fig. 3-12. The profiles of the source factors match the profile of the respective tracer compounds: toluene for traffic (Fig. 3-6), ethanol for disinfectants (Fig. 3-2), and furfural for wood combustion (Fig. 3-4). The diurnal profile of the urban background factor can be explained by reduced pollutant dispersion at night, which leads to increased levels of background pollution in the urban atmosphere (Akimoto, 2016).

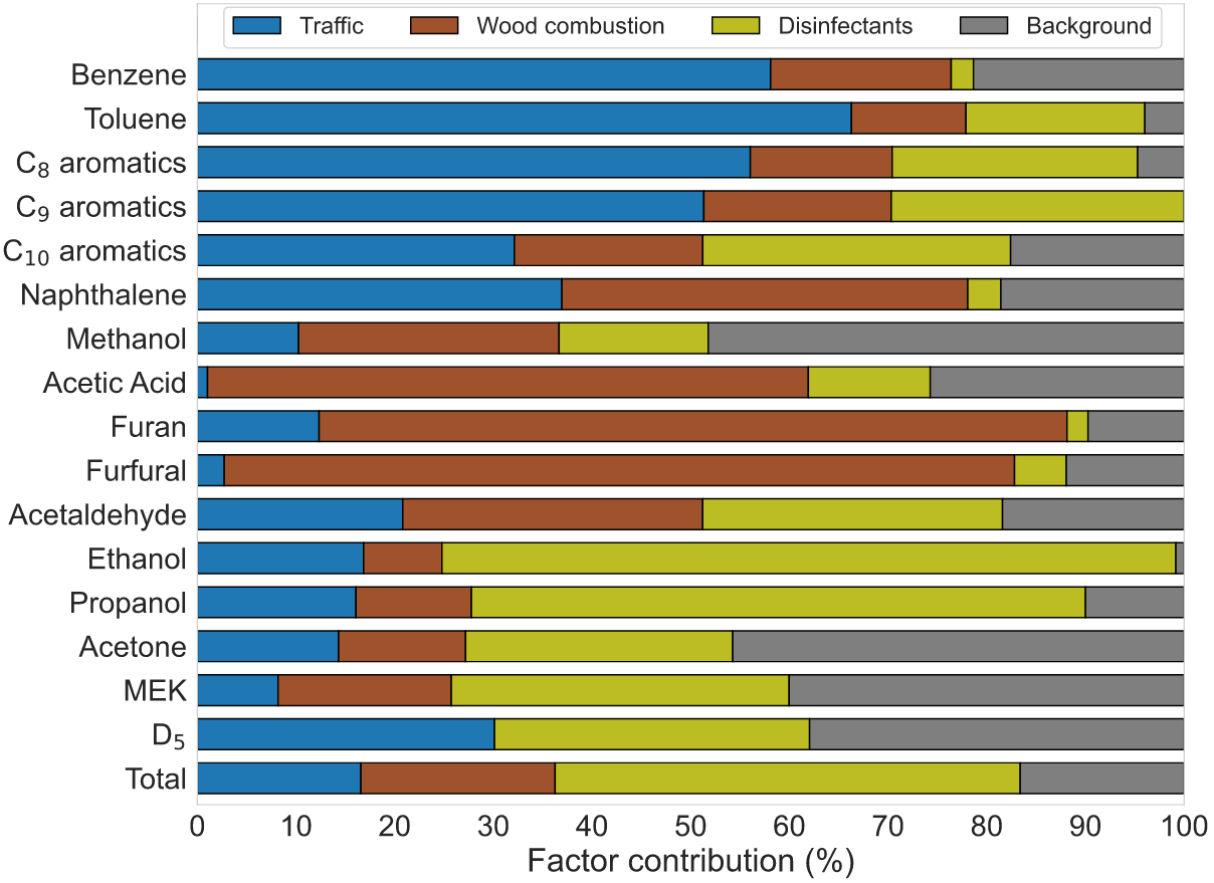

Figure 3-11: Factor contribution of each considered compound calculated by the PMF model.

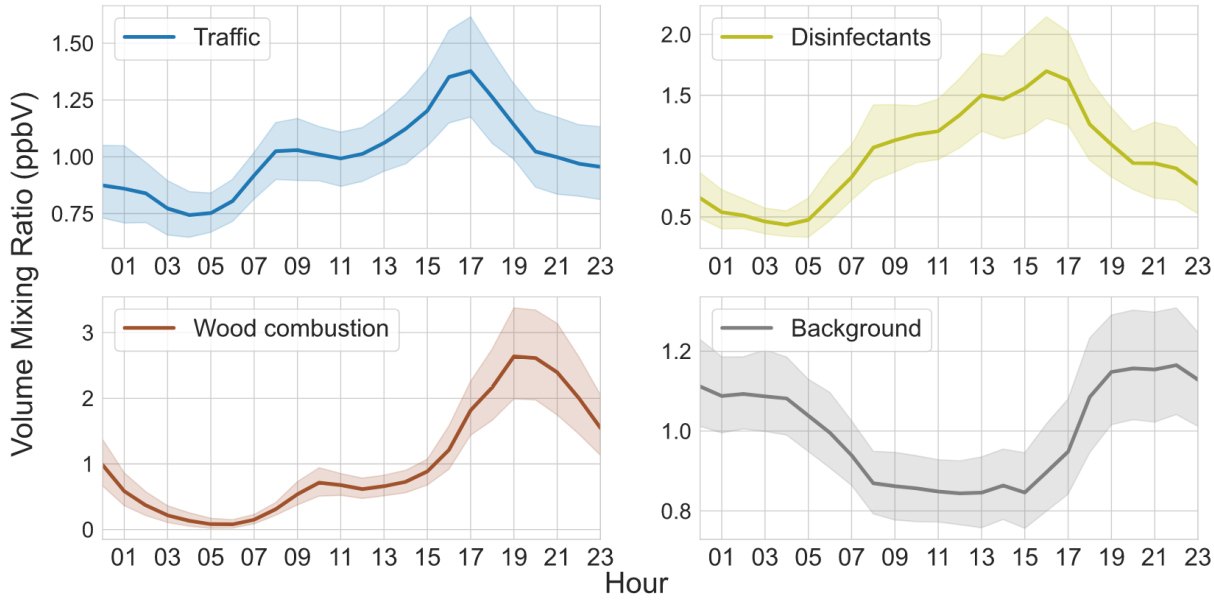

Figure 3-12: Diurnal profiles of the assigned factors.

Fig. 3-13 shows the source factor contributions to the mean VMR of each of the 16 target VOCs. The most abundant VOCs originate in disinfectant use and wood combustion. This finding indicates that traffic emissions were not the dominant source of VOCs in the urban atmosphere of Oslo, an observation that has also been made for other cities (i.e. NYC, Gkatzelis et al., 2021). The contribution of the four sources to the total VOC profile is shown in Fig. 3-14.

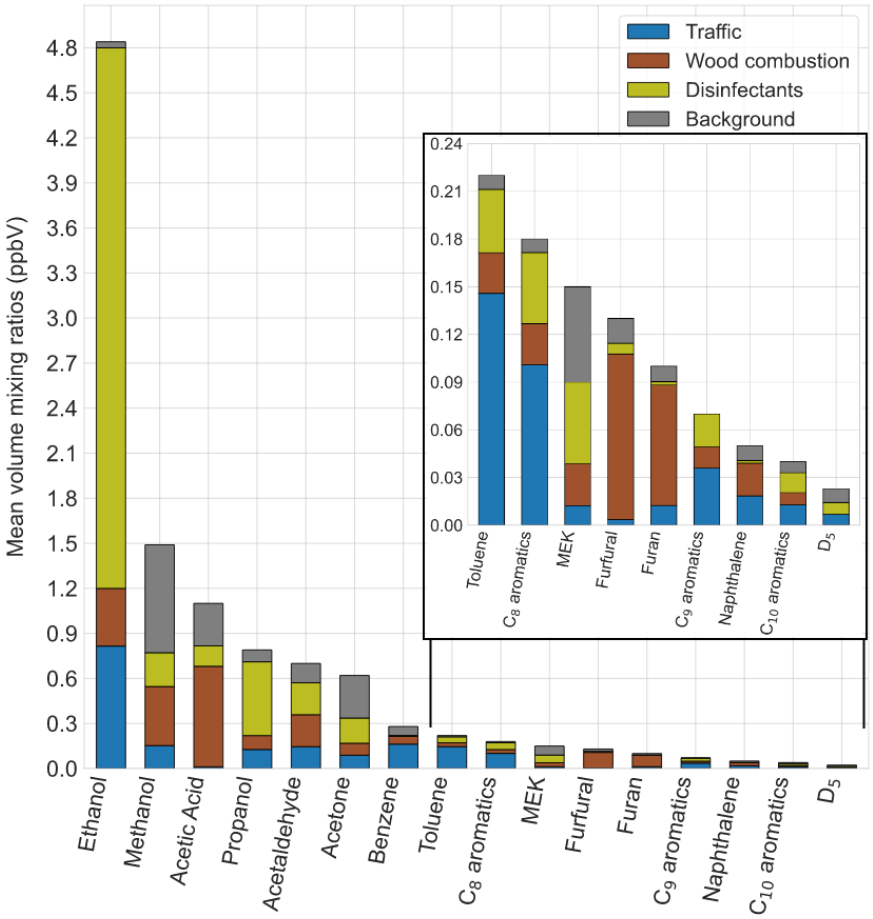

Figure 3-13: Mean VMR of the VOCs with factor apportions from the PMF analysis.

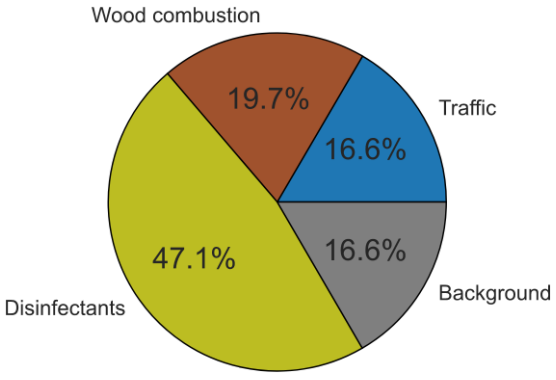

Figure 3-14: The contributions of the four factors assigned in the PMF model to the total VOC mass.

The disinfectant factor contributed to almost half of the VOC load in the urban atmosphere of Oslo, more than the traffic and wood combustion factors combined (36.3 %). While ethanol and propanol dominated the disinfectant factor, significant contributions came also from the oxidation products acetaldehyde and acetone/propanal. The most important finding from my Master's project was thus that the Covid-19 pandemic also changed the VOC composition of the urban atmosphere of Oslo. Another important finding is that the contribution from residential wood combustion source is comparable to that of the traffic source. The observation agrees with the apportionments of Baudic et al. (2016) and Languille et al. (2020), both reporting 47 % contribution from wood combustion to the total VOC emissions in French megacities during cold seasons. Importantly, 41 % of the naphthalene was apportioned to the wood combustion source. Any effort to improve the air quality in Oslo must thus consider the significant emissions of PAHs, and additional benzene from residential wood combustion.

4. Conclusion

A selection of 16 VOCs and NO_2 were monitored continuously at the centrally located Oslo Metropolitan University from 14. November 2020 to 31. January 2021. The measurements allowed evaluation of temporal variations and diurnal trends occurring during the transition to the winter season in Oslo, and during the peak of the Covid-19 pandemic. Sources were identified by the usage of tracer compounds, and furthermore by PMF modelling which also provided the respective contributions to the overall atmospheric profile of the targeted VOCs.

The measurements from OsloMet support the recent observations of traffic-related VOCs contributing with a minimal portion of the total VOCs in comparison to other emission sources in urban environments globally. The PMF model apportioned comparable amounts of VOCs to biomass combustion as for traffic. Since the measurements were performed during relatively cold temperatures, this apportion was determined to originate from residential heating by firewood combustion. More importantly, 47 % of the total VOC profile was apportioned to what was considered disinfectant usage, based on the elevated levels of both ethanol and propanols. The high apportion suggests the atmospheric composition of VOCs in Oslo was influenced by the Covid-19 pandemic through the elevated usage of hand sanitizers.

The scope of a Master's thesis added a few limitations to the analysis. Due to the small selection of VOCs, only the most prominent sources could be identified by the PMF model, made apparent by a significant apportion to a fourth, communal "background factor". Better separation could also be achieved by applying constraints to the model to separate contributions caused by aged air plumes or co-emittance with other factors. Furthermore, it would be interesting to investigate variations in the VOC profile during warmer seasons, especially the contribution from the disinfectant factor.

Finally, the thesis does not cover any eventual climate or health-related consequences related to the high alcohol levels. Thought well below occupational exposure limits, the additional VOC mass could promote formation of ground-level ozone and particles. This also applies to the comparatively high occurrence of VOCs from biomass combustion, which additionally represents a source of carcinogenic benzene, and a source of PAHs (e.g naphthalene). Overall, further monitoring of non-traffic pollutants in Oslo should be of interest following the implications of this thesis.

References

Akimoto, H. (2016). *Atmospheric Reaction Chemistry* (1 ed.). Springer. https://doi.org/10.1007/978-4-431-55870-5

Baudic, A., et al. (2016). Seasonal variability and source apportionment of volatile organic compounds (VOCs) in the Paris megacity (France). *Atmos. Chem. Phys., 16*(18), 11961-11989. https://doi.org/10.5194/acp-16-11961-2016

Bruns, E., et al. (2016). Characterization of gas-phase organics using proton transfer reaction time-of-flight mass spectrometry: fresh and aged residential wood combustion emissions. *Atmospheric Chemistry and Physics Discussions*, 1-35. https://doi.org/10.5194/acp-2016-753

Cappellin, L., et al. (2012, 2012/02/21). On Quantitative Determination of Volatile Organic Compound Concentrations Using Proton Transfer Reaction Time-of-Flight Mass Spectrometry. *Environmental Science & Technology, 46*(4), 2283-2290. https://doi.org/10.1021/es203985t

Coggon, M. M., et al. (2018, 2018/05/15). Diurnal Variability and Emission Pattern of Decamethylcyclopentasiloxane (D5) from the Application of Personal Care Products in Two North American Cities. *Environmental Science & Technology, 52*(10), 5610-5618. https://doi.org/10.1021/acs.est.8b00506

de Gouw, J., & Warneke, C. (2007). Measurements of volatile organic compounds in the earth's atmosphere using proton-transfer-reaction mass spectrometry. *Mass Spectrometry Reviews, 26*(2), 223-257. https://doi.org/10.1002/mas.20119

DESA. (2019). *World Urbanization Prospects: The 2018 Revision*. United Nations.

Edenhofer, O., et al. (2014). *IPCC, 2014: Climate Change 2014: Mitigation of Climate Change. Contribution of Working Group III to the Fifth Assessment Report of the Intergovernmental Panel on Climate Change* (C. U. Press, Ed.). Cambridge.

EEA. (2018). Fuel quality in the EU in 2016. 51. https://doi.org/10.2800/224432

Ellis, A. M., & Mayhew, C. A. (2014). *Proton Transfer Reaction Mass Spectrometry - Principles and Applicatoins* (First Edition ed.). Wiley.

Fevang, E., et al. (2021, 2021/03/01/). Who goes electric? The anatomy of electric car ownership in Norway. *Transportation Research Part D: Transport and Environment, 92*, 102727. https://doi.org/10.1016/j.trd.2021.102727

Gkatzelis, G. I., et al. (2021a, 2021/01/05). Identifying Volatile Chemical Product Tracer Compounds in U.S. Cities. *Environmental Science & Technology, 55*(1), 188-199. https://doi.org/10.1021/acs.est.0c05467

Gkatzelis, G. I., et al. (2021b, 2021/03/15). Observations Confirm that Volatile Chemical Products Are a Major Source of Petrochemical Emissions in U.S. Cities. *Environmental Science & Technology*. https://doi.org/10.1021/acs.est.0c05471

Gross, J. H. (2017). *Mass Spectrometry - A Textbook* (Third Edition ed.). Springer. https://doi.org/10.1007/978-3-319-54398-7

Guenther, A., et al. (1995, 1995/05/20). A global model of natural volatile organic compound emissions [https://doi.org/10.1029/94JD02950]. *Journal of Geophysical Research: Atmospheres, 100*(D5), 8873-8892. https://doi.org/10.1029/94JD02950

Ionicon. (2021). *Liquid Calibration Unit*. Retrieved 25.04.2021 from https://www.ionicon.com/accessories/details/liquid-calibration-unit-lcu

Ito, K., et al. (2004, 2004/10/01/). Spatial variation of PM2.5 chemical species and source-apportioned mass concentrations in New York City. *Atmospheric Environment, 38*(31), 5269-5282. https://doi.org/10.1016/j.atmosenv.2004.02.063

Languille, B., et al. (2020, 2020/04/01/). Wood burning: A major source of Volatile Organic Compounds during wintertime in the Paris region. *Science of The Total Environment, 711*, 135055. https://doi.org/10.1016/j.scitotenv.2019.135055

López-Aparicio, S., et al. (2017, 2017/04/15/). Public participation GIS for improving wood burning emissions from residential heating and urban environmental management. *Journal of Environmental Management, 191*, 179-188. https://doi.org/10.1016/j.jenvman.2017.01.018

Miljødirektoratet. (2021). *Siloksaner*. Retrieved 25.04.2021 from https://miljostatus.miljodirektoratet.no/tema/miljogifter/prioriterte-miljogifter/siloksaner/

Norris, G., & Duvall, R. (2014). EPA Positive Matrix Factorization (PMF) 5.0 - Fundamental and User Guide.

Paatero, P., & Tapper, U. (1994). Positive matrix factorization: A non-negative factor model with optimal utilization of error estimates of data values. *Environmetrics, 5*(2), 111-126. https://doi.org/10.1002/env.3170050203

Rantala, P., et al. (2016). Anthropogenic and biogenic influence on VOC fluxes at an urban background site in Helsinki, Finland. *Atmos. Chem. Phys., 16*(12), 7981-8007. https://doi.org/10.5194/acp-16-7981-2016

Sousa Santos, G., et al. (2020, 2020/12/01/). Evaluation of traffic control measures in Oslo region and its effect on current air quality policies in Norway. *Transport Policy, 99*, 251-261. https://doi.org/10.1016/j.tranpol.2020.08.025

SSB. (2021). *Kommunefakta - Oslo*. Retrieved 26.04.2021 from https://www.ssb.no/kommunefakta/oslo

TAPI. (2014). Model T500U CAPS NO2 Analyzer - Operation Manual. 213 - 214.

Tsai, P.-J., et al. (2001, 2001/10/20/). Health-risk assessment for workers exposed to polycyclic aromatic hydrocarbons (PAHs) in a carbon black manufacturing industry. *Science of The Total Environment, 278*(1), 137-150. https://doi.org/10.1016/S0048-9697(01)00643-X

Wang, J., et al. (1995, 1995/12/01). Evaluation of Ethanol, 1-Propanol, and 2-Propanol in a Direct Oxidation Polymer-Electrolyte Fuel Cell: A Real-Time Mass Spectrometry Study. *Journal of The Electrochemical Society, 142*(12), 4218-4224. https://doi.org/10.1149/1.2048487

Wild, C., et al. (2020). *World Cancer Report: Cancer Research for Cancer Prevention*. IARC.

Yuan, B., et al. (2017, 2017/11/08). Proton-Transfer-Reaction Mass Spectrometry: Applications in Atmospheric Sciences. *Chemical Reviews, 117*(21), 13187-13229. https://doi.org/10.1021/acs.chemrev.7b00325

Appendix

A. Tables

A-1: Occupational Exposure Limits for some of the target VOCs available from of various agencies.

Compound	Long-term exposure limit (ppm)	Short-term exposure limit (ppm)	Agency
Methanol	200.0	-	EU
Acetaldehyde	200.0	200	OSHA
Ethanol	1000.0	-	OSHA
Acetic Acid	10	15	NIOSH
MEK	200.0	300.0	EU
Benzene	1.0	-	EU
Ethyl Acetate	200.0	400.0	EU
Toluene	50.0	100.0	EU
Xylene	50.0	100.0	EU
TMB	20.0	-	EU
Naphthalene	10.0	-	EU
NO_2	0.5	1.0	EU

A-2: Volume mixing ratios of VOCs in cal-gas.

Compound	Volume Mixing Ratio (ppbV)	Uncertainty*
Formaldehyde	10099	± 5 %
Propene	9943	± 5 %
Acetaldehyde	1040	± 5 %
Methanol	1193	± 5 %
Acetonitrile	1062	± 5 %
Acetone	1035	± 5 %
Isoprene	970	± 5 %
DMS	973	± 5 %
Methyl Ethyl Ketone	984	± 5 %
Benzene	1022	± 5 %
Toluene	1011	± 5 %
C_8-aromatics	988	± 5 %
α-Pinene	923	± 5 %
C_9-aromatics	935	± 5 %
D_5	4426	± 5 %

* Estimate of the combined uncertainties of the gravimetric preparation and analysis

Table A-3: Data coverage of PTR-ToF-MS

Green = 20+ hours of data; Blue = 10-19 hours of data; Red = Less than 9 hours of data.

	Monday	Tuesday	Wednesday	Thursday	Friday	Saturday	Sunday
Week 46 - 2020							
Week 47 - 2020							
Week 48 - 2020							
Week 49 - 2020							
Week 50 - 2020							
Week 51 - 2020							
Week 52 - 2020							
Week 53 - 2020							
Week 1 - 2021							
Week 2 - 2021							
Week 3 - 2021							
Week 4 - 2021							

Missing data was caused by maintenance or instrumental issues occurring at three occasions.

Table A-4: Data coverage of NO_2-analyzer

Green = 20+ hours of data; Blue = 10-19 hours of data; Red = Less than 9 hours of data.

	Monday	Tuesday	Wednesday	Thursday	Friday	Saturday	Sunday
Week 46 - 2020							
Week 47 - 2020							
Week 48 - 2020							
Week 49 - 2020							
Week 50 - 2020							
Week 51 - 2020							
Week 52 - 2020							
Week 53 - 2020							
Week 1 - 2021							
Week 2 - 2021							
Week 3 - 2021							
Week 4 - 2021							

Missing data in week 2-4 was caused by an issue with the instrument's data synchronization.

B. Equations

Reduced electric field, E/N (Ellis & Mayhew, 2014)

$$\frac{E}{N} = \frac{V}{d} \cdot \frac{V_M}{N_A} \cdot \frac{T_d}{273.15} \cdot \frac{101.325}{P_d} \quad \text{(B-1)}$$

V = Potential difference between electrodes (V)

d = distance between electrodes/plates in DT (cm)

V_M = Molar volume of ideal gas = 22414 cm^3 mol^{-1}

N_A = Avogadros' number = $6.022 \cdot 10^{23}$ mol^{-1}

Td = Operational temperature of DT (K)

P_d = Operational pressure of DT (kPa)

Beer's law (TAPI, 2014)

$$A = \varepsilon \cdot l \cdot c \quad \text{(B-2)}$$

A = Absorbance,

ε = Molar absorptivity

l = Mean path length

c = concentration of absorbing gas

Conversion to µg/m^3

$$\mu g m^{-3}(i) = ppbv(i) \cdot \frac{m}{z}(i) \cdot \frac{P}{T} \quad \text{(B-3)}$$

P = atmospheric pressure. Standard value = 1

T = ambient temperature. Standard value = 25 °C

C. Figures

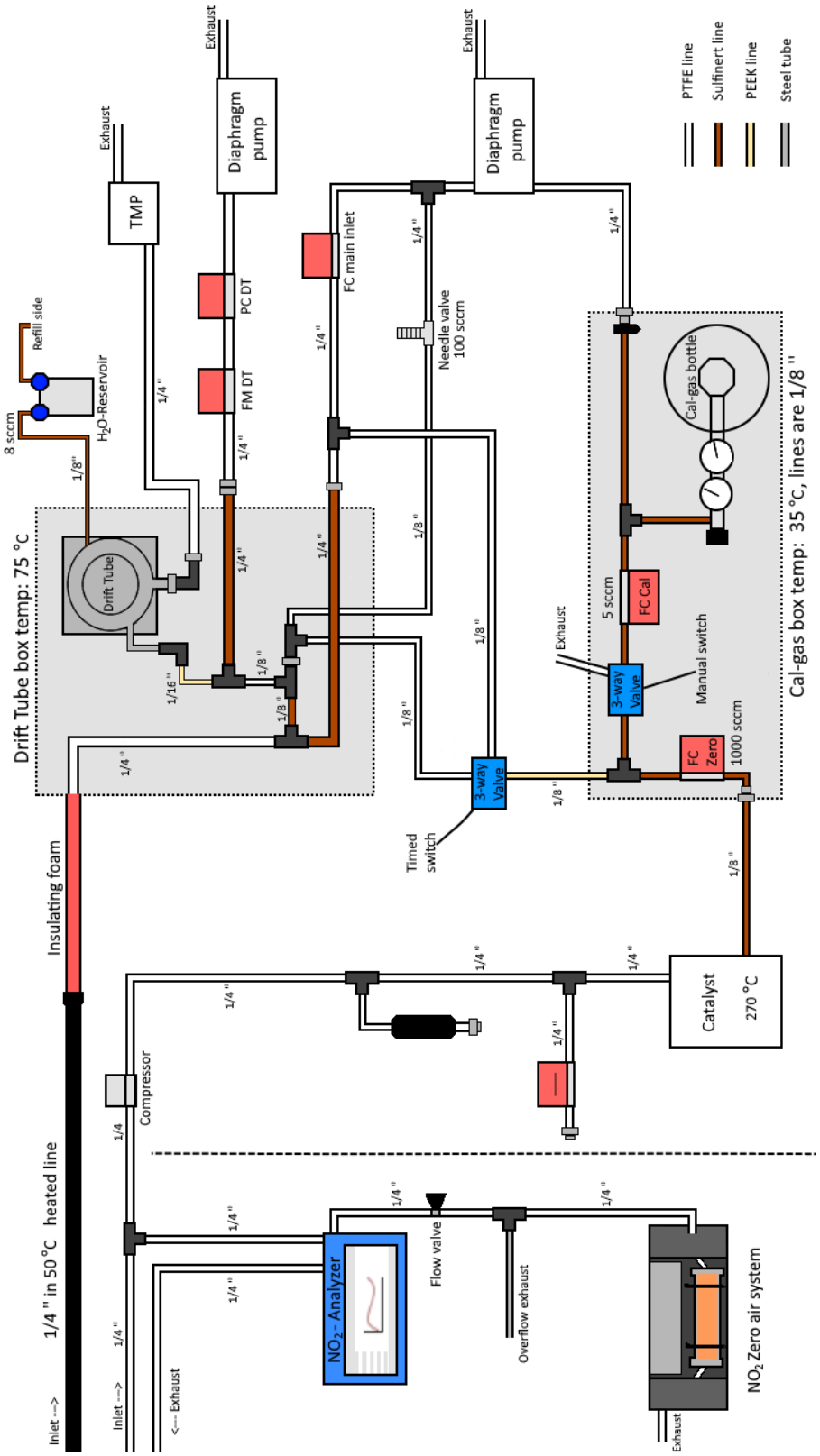

Figure C-1: Detailed overview of total inlet setup of both the PTR-ToF-MS and the NO_2-analyzer as constructed at the measurement site.

D. Sample preparation

D-1 shows the formula of how much gram analyte must be weighted in per litre of solvent to obtain a set VMR. D-1 is based on the mol/L to ppbV conversion formula provided by Ionicon, the manufacturer of the LCU unit.

$$\frac{g\ (analyte)}{L\ (solvent)} = \frac{VMR\ (ppbV)\ \cdot 10^{-9}}{LCU\ liquid\ flow\ (\mu L/min)}\ \cdot\ \frac{LCU\ stanard\ gas\ flow\ (\mu L/min)}{Molar\ volume\ of\ ideal\ gas\ (\frac{L}{mol})}\ \cdot\ Mw_{analyte}\left(\frac{g}{mol}\right) \qquad \text{(D-1)}$$

Since the samples were alcohols, liquids at room temperature, the result using eq. D-1 were divided by their respective densities to obtain how many mL to mix into the standards.

Directly measuring to 10 ppb solutions are difficult because it would require exceedingly small volumes of analyte. Therefore, 10 ppmV (10 000 ppbV) solutions were prepared. The final 10 ppbV solution could then be obtained by mixing 1 mL of the ppmV solution into new 1 L solutions, diluting by a factor of 1000.

Ethanol calculations

Mw = 46.07 g/mol ρ = 0.789 g/mL

$$\frac{g}{L}(Ethanol) = \frac{10\ 000\ ppbV\ \cdot\ 10^{-9}}{10\ sccm}\ \cdot\ \frac{10^{6}\ sccm}{22.4\frac{L}{mol}}\ \cdot 46.019\frac{g}{mol}\ = 2.05\frac{g}{L} \qquad \text{(D-2a)}$$

$$\frac{mL}{L}\ (Ethanol) = \frac{0.912\ g\ /\ L}{0.789\ g\ /\ mL}\ =\ \mathbf{2.61\ mL/L} \qquad \text{(D-2b)}$$

2-Propanol calculations

Mw = 60.096 g/mol ρ = 0.786 g/mL

$$\frac{g}{L}(Propanol) = \frac{10\ 000\ ppbV \cdot 10^{-9}}{10\ sccm} \cdot \frac{10^6\ sccm}{22.4\frac{L}{mol}} \cdot 60.096\frac{g}{mol} = 2.68\frac{g}{L} \quad \text{(D-3a)}$$

$$\frac{mL}{L}\ (Propanol) = \frac{0.912\ g/\ L}{0.786\ g\ /\ mL} = \mathbf{3.41\ mL/L} \quad \text{(D-3b)}$$

E. Calculation of mass accuracies

The relative mass accuracy is a measure of how close the experimentally assigned masses (accurate *m/z*) are to the theoretically exact *m/z*. It is calculated by:

$$rel.\ mass\ accuracy = 10^6 \cdot \frac{m/z\ (exact) - m/z\ (measured)}{m/z\ (exact)} \qquad \text{(E-1)}$$

Due to the length of the campaign, the raw data was separated into four merges. Each merge went through individual peak fitting processes, consequently leading to slight variations in the accurate *m/z* for the overall dataset. Following this, Table E-1 below presents the mean accurate *m/z* and the mean relative mass accuracies with their respective ranges:

Table E-1: Summary of accurate and exact *m/z* of protonated VOCs, and their relative mass accuracies

Compound	Accurate protonated *m/z*	Exact protonated *m/z*	Relative accuracy (ppm)
H_3O^+	21.022 ± 0.000	21.022	6 ± 6
Methanol	33.033 ± 0.000	33.033	- 26 ± 12
$H_3O^+(H_2O)$	38.033 ± 0.000	38.034	-20 ± 4
Propanol	41.041 ± 0.001	41.041	50 ± 14
Acetaldehyde	45.033 ± 0.000	43.054	52 ± 11
Ethanol	47.051 ± 0.000	47.049	47 ± 4
Acetic Acid	61.031 ± 0.000	61.028	42 ± 6
Furan	69.035 ± 0.001	69.033	26 ± 10
Methyl Ethyl Ketone	73.064 ± 0.003	73.065	- 6 ± 43
Benzene	79.056 ± 0.002	79.054	27 ± 22
Toluene	93.071 ± 0.002	93.070	13 ± 16
Furfural	97.032 ± 0.001	97.028	33 ± 9
C_8-aromatics	107.087 ± 0.000	107.086	17 ± 17
C_9-aromatics	121.101 ± 0.000	121.101	0 ± 0
Naphthalene	129.070 ± 0.001	129.070	0 ± 10
C_{10}-aromatics	135.117 ± 0.000	135.117	- 1 ± 1
D_5	371.096 ± 0.000	371.101	- 14 ± 14